NOAA Atlas NESDIS 15

SEASONAL VARIABILITY OF DYNAMIC HEIGHT AND ITS FOURIER ANALYSIS

Washington, D.C.
July 1997

U.S. DEPARTMENT OF COMMERCE
National Oceanic and Atmospheric Administration
National Environmental Satellite, Data, and Information Service

NOAA Atlas NESDIS 15

SEASONAL VARIABILITY OF DYNAMIC HEIGHT AND ITS FOURIER ANALYSIS

Sydney Levitus, Grigory Isayev Monterey and Timothy Boyer
National Oceanographic Data Center
Ocean Climate Laboratory
Silver Spring, Maryland 20910

Washington, D.C.
July 1997

U.S. DEPARTMENT OF COMMERCE
William M. Daley, Secretary

National Oceanic and Atmospheric Administration
D. James Baker, Under Secretary

National Environmental Satellite, Data, and Information Service
Robert S. Winokur, Assistant Administrator

National Oceanographic Data Center
USER SERVICES

Additional copies of this publication, as well as information about NODC data holdings, products, and services, are available on request directly from the NODC. NODC information and data are also available over the Internet through the NODC World Wide Web and Gopher sites.

National Oceanographic Data Center
User Services Branch
NOAA/NESDIS E/OC1
SSMC3, 4th Floor
1315 East-West Highway
Silver Spring, MD 20910-3282

Telephone: (301) 713-3277

Fax: (301) 713-3302

E-mail: services@nodc.noaa.gov

NODC World Wide Web site: http://www.nodc.noaa.gov/

NODC Gopher site: gopher.nodc.noaa.gov

Contents

Acknowledgments vi

Abstract 1

1. Introduction 1

2. Data 2

3. Computational Formula 3

4. Fourier Decomposition 3

5. Results 4
   5.1 Global distribution 4
   5.2 Global and basin zonal averages 5

6. Summary 6

7. References 7

List of Figures

Figure A1 January mean dynamic height (dynamic-cm) 0-1000 m.
Figure A2 February mean dynamic height (dynamic-cm) 0-1000 m.
Figure A3 March mean dynamic height (dynamic-cm) 0-1000 m.
Figure A4 April mean dynamic height (dynamic-cm) 0-1000 m.
Figure A5 May mean dynamic height (dynamic-cm) 0-1000 m.
Figure A6 June mean dynamic height (dynamic-cm) 0-1000 m.
Figure A7 July mean dynamic height (dynamic-cm) 0-1000 m.
Figure A8 August mean dynamic height (dynamic-cm) 0-1000 m.
Figure A9 September mean dynamic height (dynamic-cm) 0-1000 m.
Figure A10 October mean dynamic height (dynamic-cm) 0-1000 m.
Figure A11 November mean dynamic height (dynamic-cm) 0-1000 m.
Figure A12 December mean dynamic height (dynamic-cm) 0-1000 m.
Figure A13 Annual mean dynamic height (dynamic-cm) 0-1000 m.

Figure B1 January mean minus annual mean dynamic height (dynamic-cm) 0-1000 m.
Figure B2 February mean minus annual mean dynamic height (dynamic-cm) 0-1000 m.
Figure B3 March mean minus annual mean dynamic height (dynamic-cm) 0-1000 m.
Figure B4 April mean minus annual mean dynamic height (dynamic-cm) 0-1000 m.
Figure B5 May mean minus annual mean dynamic height (dynamic-cm) 0-1000 m.
Figure B6 June mean minus annual mean dynamic height (dynamic-cm) 0-1000 m.
Figure B7 July mean minus annual mean dynamic height (dynamic-cm) 0-1000 m.
Figure B8 August mean minus annual mean dynamic height (dynamic-cm) 0-1000 m.
Figure B9 September mean minus annual mean dynamic height (dynamic-cm) 0-1000 m.
Figure B10 October mean minus annual mean dynamic height (dynamic-cm) 0-1000 m.
Figure B11 November mean minus annual mean dynamic height (dynamic-cm) 0-1000 m.
Figure B12 December mean minus annual mean dynamic height (dynamic-cm) 0-1000 m.

Figure C1 Amplitude (dynamic-cm) of the first harmonic.
Figure C2 Percent variance contributed by the first harmonic.
Figure C3 Phase (months) of the first harmonic.
Figure C4 Zonally averaged annual mean dynamic height (dynamic-cm) (0-1000) m for the global ocean and individual ocean basins.
Figure C5 Zonally averaged amplitude (dynamic-cm) of the first harmonic of the climatological annual cycle of dynamic height (0-1000) m for the global ocean and individual ocean basins.
Figure C6 Zonally averaged phase (months) of the first harmonic of the climatological annual cycle of dynamic height (0-1000) m for the global ocean and individual ocean basins.
Figure C7 Zonally averaged percent variance contributed by the first harmonic to the climatological annual cycle of dynamic height (0-1000) m for the global ocean and individual ocean basins.
Figure C8 Amplitude (dynamic-cm) of the second harmonic.
Figure C9 Percent variance contributed by the second harmonic.
Figure C10 Zonally averaged amplitude (dynamic-cm) of the second harmonic of the climatological annual cycle of dynamic height (0-1000) m for the global ocean and individual ocean basins.
Figure C11 Zonally averaged phase (months) of the second harmonic of the climatological annual cycle of dynamic height (0-1000) m for the global ocean and individual ocean basins.
Figure C12 Zonally averaged percent variance contributed by the second harmonic of the climatological annual cycle of dynamic height (0-1000) m for the global ocean and individual ocean basins.

Figure D1 Hemispheric averages of TOPEX altimeter monthly sea level anomaly (forty-one months) and climatological monthly steric sea level anomaly (deviation from annual mean).

Acknowledgments

Substantial amounts of historical oceanographic data used in this study were located and digitized (Data Archaeology and Rescue projects) with funding from the NOAA Climate and Global Change Program and the NOAA Environmental Services Data and Information Management Program.

The work described in this atlas was made possible by the efforts of scientists, technicians, ships' crew, data managers, and science administrators from the international scientific community. This atlas represents the results of several different research/data management projects of the NODC Ocean Climate Laboratory at the National Oceanographic Data Center (NODC) and World Data Center-A (WDC-A) for Oceanography. The products in this atlas are all based on the master oceanographic data archives maintained by NODC/WDC-A as well as data acquired as a result of the IOC/IODE Global Oceanographic Data Archaeology and Rescue (GODAR) project. These archives and data sets exist because scientists and data managers of the international scientific community have submitted these data to national and regional data centers. In turn, these centers have submitted data to the World Data Center system established under the International Council of Scientific Unions (ICSU) and the Intergovernmental Oceanographic Commission (IOC). This atlas and similar works would not exist without these international efforts. In particular, we would like to thank data managers at these centers and the administrators and staff at all of these organizations.

The archiving of oceanographic data at international data centers means that the substantial expenditures in human and capital resources devoted to oceanographic measurement programs will be fully exploited, both for present and future scientific studies. Many of the data have been collected for diverse purposes but when combined in a uniform database provide most of our knowledge of property distributions in the world ocean for both climatological averaging periods as well as for the temporal variability of these properties.

The data sets and products represented by this atlas are being distributed internationally without restriction in accordance with ICSU/IOC data management policies and U.S. Climate and Global Change policy in support of Global Change Research.

John Lillibridge, Chet Koblinsky, and John Antonov provided valuable comments about the original version of this manuscript.

SEASONAL VARIABILITY OF DYNAMIC HEIGHT AND ITS FOURIER ANALYSIS

Sydney Levitus, Grigory Isayev Monterey, and Timothy Boyer
Ocean Climate Laboratory
National Oceanographic Data Center
Silver Spring, Maryland

ABSTRACT

This atlas contains maps of climatological monthly mean dynamic height (dynamic-cm) of the sea surface relative to the 1000 m depth level, their deviations from their climatological annual mean, and results of their Fourier analysis. The latter includes geographical distributions of amplitudes and phases of the first and second Fourier harmonics, and percent variance contributed by these harmonics to the climatological annual cycle. Zonal averages of these quantities over 1^0 latitude belts, both for the global ocean and for the individual ocean basins, are presented.

1. INTRODUCTION

The study of sea level and its variability is a subject of great importance. Knowledge of the general circulation statistics of the world ocean, which includes sea level statistics, is critical to describing the role of the world ocean as part of the earth's climate system. The annual cycle of sea level and its interannual variability yields information concerning the dynamics of ocean currents as well as the interannual, integrated variability of temperature and salinity. For example, Montgomery (1938) related fluctuations in sea level from tide gauge stations along the east coast of the United States to fluctuations in dynamic heights associated with ocean currents. He referred to earlier work by Sandstrom (1903) as the first attempt to relate changes in sea level to ocean currents.

More recently the study of sea level has become a topic of great interest from the point of view of climate change, particularly the response of the Earth's climate system to possible warming of the atmosphere troposphere an d ocean due to the increased concentration of atmospheric CO_2 and other radiatively important gases. Barnett (1983), Douglas (1991,1992), and Gornitz (1995) have studied the temporal variability and climatic chamge of sea level based on tide gauge measurements. Possible changes in sea level due to anthropogenic effects such as increasing atmosphere CO_2 are of obvious socioeconomic importance because of the obvious consequences of sea level for coastal regions.

Changes in sea level are closely linked to variability in geophysical quantities of interest to many scientific disciplines. For example, Munk and Revelle (1952) compared historical observation of changes in the length-of-day to changes in steric sea level induced by temperature changes, as well as sea level changes induced by ice cap melting and deformation of the earth's crust. Munk and MacDonald (1960) and Lambeck (1980) discuss some of these effects in more detail.

Patullo *et al.* (1955) introduced the term "steric sea level" to distinguish that portion of temporally varying sea level that arises due to changes in the temperature and/or salinity of a water column. For example, an increase in temperature or decrease in salinity of a water column will increase the height of the column. Through recent usage, the term "steric sea level" is now used interchangeably with dynamic height and geopotential thickness. Previous

works describing this parameter are relatively limited and usually encompass the presentation of monthly or seasonal distributions of sea level for limited parts of ocean basins, but in a few cases, include entire ocean basins. For example, Wyrtki (1971, 1975) produced monthly distributions of steric sea level for the Indian and Pacific Oceans.

Patullo *et al.* (1955) made a comprehensive study of the climatological annual cycle of sea level at tide-gauge stations from various locations around the globe (mainly coastal) and compared these records with the annual cycle of steric sea level from historical hydrographic data. Their study included determining the relative roles of the annual cycles of temperature and salinity in determining the annual cycle of steric sea level. Much of this earlier work was reviewed by Lisitzin (1974). Hicks *et al.* (1983) and Woodworth (1984) have updated our knowledge of the annual cycle of sea level using tide-gauge measurements at various locations along the coasts of the United States and the world ocean, respectively.

There have been several attempts to model the annual cycle of sea level over the last twenty five years. The basic processes that produce the annual cycle in both tropical- and mid-latitudes are fairly well understood. Gill and Niiler (1973) used a set of simple diagnostic equations with climatological forcing to study the annual cycle at mid-latitudes in the North Pacific and North Atlantic. Their model results show that in both the North Pacific and the North Atlantic oceans, the upper ocean steric level and the inverted barometric response to atmospheric loading are the dominant factors in mid-latitude sea level variations. The air-sea heat flux is the main contributor to variations in mid-latitude steric level change on an annual time-scale. Their model produces sizeable east/west variations, as well. A major cause in the zonal variation of mid-latitude sea level is the much more dramatic air-sea heat flux variations in the western ocean basins resulting from the sensible heat flux between relatively warm waters and winter outbreaks of cold, dry continental polar air masses that is strongly effected by the adjacent continental land mass. In mid-latitudes, the response to variations in surface heat flux is local because the ocean wave modes are too sluggish to respond at this frequency. However, seasonal variations of the western boundary currents (e.g. Fu *et al.*, 1987) caused by other processes (Anderson and Cory, 1985; Greatbatch and Goulding, 1989) may also be substantial. In tropical latitudes, ocean wave modes respond at much higher frequencies (e.g. Philander, 1978) and substantial upper ocean sea level fluctuations could be caused by the seasonal redistributions of the wind fields. In the tropical Atlantic, for example, Merle (1980) has shown that the annual variation in upper ocean heat content is ten times larger than the air-sea heat exchange. These changes in upper ocean steric level are dominated by fluctuations of the thermocline and represent the wind forced response of the tropical ocean.

Satellite altimetry is now greatly contributing to our understanding of sea level and the general circulation of the world ocean. The ongoing US/France *TOPEX/POSEIDON* (T/P) project is the first global observing system specifically designed to study large-scale ocean dynamics. References to papers on seasonal to interannual variability of global sea level based on T/P altimetry can be found in recent review by Fu et al. (1996). Many of these papers were published in two special issues of the *Journal of Geophysical Research* (1994, Vol. 99, No. C12; 1995, Vol. 100, No. C12). Cheney *et al.* (1994) and Nerem *et al.* (1994) presented spatial distributions of amplitude and phase of annual and semiannual variations of the T/P altimetry derived global sea level and compared them to the corresponding parameters derived from temperature-salinity fields presented by Levitus (1982). Chao and Fu (1995) compared the T/P derived and OGCM (ocean general circulation model) derived amplitude and phase of the annual cycle of global sea level.

The purpose of this atlas is to document the climatological annual cycle of dynamic height (0-1000 m) derived from climatological hydrographic data. Objectively analyzed climatological monthly mean fields of temperature and salinity are used to compute climatological monthly mean density fields and climatological monthly mean fields of dynamic height of the ocean surface relative to the 1000 m depth level for the World Ocean. We present the global climatological monthly mean fields of dynamic height, their deviations from the annual mean, and the results of their Fourier analysis (amplitudes and phases of first and second Fourier harmonics, etc.).

2. DATA

As a result of the Intergovernmental Oceanographic Commission (IOC) Global Oceanographic Data Archeology and Rescue (GODAR) project (Levitus *et al.*, 1994a), an updated temperature and salinity database for the World Ocean has been compiled at the National Oceanographic Data Center. Climatological monthly

mean temperature and salinity fields based on this database were used to compute climatological monthly mean density fields and the climatological monthly mean dynamic heights of the World Ocean surface relative to the 1000 m depth level. The fields are defined on a $1^0 \times 1^0$ grid at 19 standard levels from the ocean surface to 1000 m depth. These fields are described in detail by Levitus and Boyer (1994b) and Levitus *et al.* (1994c). Climatological monthly mean density fields are computed based on the International Equation of State of sea water.

3. COMPUTATIONAL FORMULAS

Geopotential thickness, ΔD, between two isobaric surfaces p_1 and p_2 in the ocean is defined as

$$\Delta D = \int_{p_1}^{p_2} \delta \, dp \qquad (1)$$

$$\delta = \alpha(S, T, p) - \alpha(35pss, 0^0C, p) \qquad (2)$$

where δ is the specific volume anomaly (Neumann and Pierson, 1966; Gill, 1982). Specific volume $\alpha(S,T,p) = \rho^{-1}(S,T,p)$ where ρ is the density, S the salinity, T the temperature, p the pressure. Using salinity in units of pss (practical salinity scale), temperature (^{0}C), and pressure (decibars), one obtains density (kg · m^{-3}) and consequently the geopotential thickness ($m^2 \circ sec^{-2}$). Assuming a hydrostatic ocean, the pressure differential in formula (1) is replaced by $\rho_0 g dz$ in which ρ_0 is a representative constant density of 1020 kg·m^{-3}, g = 9.87 m·sec^{-2} Pressure limits p_1 , p_2 in decibars are replaced by depth in meters (the justification of this approximation can be found in the monograph by Gill (1982).

The dynamic height, H, of the ocean surface relative to the 1000 m level is computed as

$$H = \rho_0 g \int_{-1000m}^{0} \delta \, dz \qquad (3)$$

4. FOURIER DECOMPOSITION

Dynamic height at every spatial grid point is represented in a form of Fourier decomposition in time (Cartwright, 1990)

$$H(t) = H_{mean} + \sum_{n=1}^{\infty} \left(A_n \cos\left(\frac{2\pi n t}{T}\right) + B_n \sin\left(\frac{2\pi n t}{T}\right) \right) \qquad (4)$$

or equivalently

$$H(t) = H_{mean} + \sum_{n=1}^{\infty} C_n \cos\left(\frac{2\pi n t}{T} + \phi_n\right) \qquad (5)$$

where T = 12 months is the period of annual cycle,

$$H_{mean} = \frac{1}{T} \int_0^T H(t) \, dt \qquad (6)$$

is the climatological annual mean dynamic height,

$$A_n = \frac{2}{T} \int_0^T H(t) \cos\left(\frac{2\pi n t}{T}\right) dt \qquad (7)$$

$$B_n = \frac{2}{T} \int_0^T H(t) \sin\left(\frac{2\pi n t}{T}\right) dt \qquad (8)$$

the following finite-difference approximations are used for H_{mean} , A_n , B_n ,

$$H_{mean} = \frac{1}{T} \sum_{i=1}^{12} H_i \Delta t \qquad (9)$$

$$A_n = \frac{2}{T} \sum_{i=1}^{12} H_i \cos\left(\frac{2\pi n i \Delta t}{T}\right) \Delta t \qquad (10)$$

$$B_n = \frac{2}{T} \sum_{i=1}^{12} H_i \sin\left(\frac{2\pi n i \Delta t}{T}\right) \Delta t \qquad (11)$$

where H_i , I = 1,.. 12, are 12 climatological monthly mean values of dynamic height, time step Δt = 1 month, period T = 12 months.

Fourier decomposition (4)-(11) determines amplitudes

$$C_n = \left(A_n^2 + B_n^2\right)^{1/2} \qquad \textbf{(12)}$$

and phases

$$\phi_n = \arccos(A_n / C_n) \qquad \textbf{(13)}$$

of Fourier harmonics.

A smoothed dynamic height H(t) at each spatial gridpoint is computed by retaining H_{mean}, and the first two Fourier harmonics.

Percent variance, V_n , contributed by the nth Fourier harmonic to the climatological annual cycle of dynamic height 0 - 1000 m is determined by the formula

$$V_n = \frac{C_n^2}{2D} \qquad \textbf{(14)}$$

$$D = \frac{1}{T}\sum_{i=1}^{12}\left(H_i - H_{mean}\right)^2 \qquad \textbf{(15)}$$

where D is the dispersion of climatological monthly mean dynamic heights H_i , I = 1 ,...12 : The derivation of formula (15) is based on the Parseval theorem. It can be found in the work by Chatfield (1989).

5. RESULTS

In all of the following figures dark shading shows areas where ocean depth is less than 1000 m; 'L' marks the location of minimum value, 'H' marks the location of maximum value of a parameter under consideration.

5.1. Global distributions

Figs. A1-A12 show monthly mean fields of dynamic height 0-1000 m obtained from the climatological monthly mean fields by retaining only the annual mean and first two Fourier harmonics. Fig. A13 shows the climatological annual mean field of dynamic height 0-1000 m. Similar fields have been presented previously (Stommel, 1964; Levitus, 1982) and the main features are well known. Relatively strong gradients define the interface between the subtropical and subpolar gyres, however, these gradients are not nearly as strong as gradients exhibited by synoptic distributions of these features. Nor are they as strong as the corresponding features found in the high resolution analyses presented by Boyer and Levitus (1997). Other major features include gradients associated with the Antarctic Circumpolar Current and with the equatorial current-countercurrent systems.

Figs. B1-B12 show the climatological monthly mean minus the climatological annual mean fields of dynamic height 0 - 1000 m. The seasonal variability of steric sea level associated with the annual temperature cycle dominates the midlatitude signal. In the tropics the annual cycle of steric sea level is dominated by thermocline displacements associated with changes in the wind and current field.

Figs. C1-C12 show the results of a Fourier analysis of dynamic height. Fig. C1 shows the amplitude of the first Fourier harmonic of the climatological annual cycle of dynamic height defined by formulae (10)-(12). One of the characteristics of Fig. C1 is that the southern hemisphere field is relatively noisy compared to the northern hemisphere field. This is most likely due to the relative paucity of data in the southern hemisphere. It is the noisiness in the climatological monthly mean fields that leads us to present these fields in a smoothed form constructed as the annual mean plus first two fourier harmonics. Major features of Fig. C1 for the northern hemisphere include the relative maxima (values exceeding 12.5 dynamic-cm) in the midlatitudes of the western Pacific and western Atlantic Oceans. These maxima are located in the same regions as maxima in the rate of climatological change of heat storage (Levitus, 1987). Thus the annual cycle of steric sea level may in part be accounted for by the annual cycle of heat storage in these regions, as noted earlier by Patullo *et al.* (1955). In the tropical Atlantic Ocean seasonal variations of dynamic height exceed 5 dynamic-cm. This is the same region where minimum changes in heat storage occur (Levitus, 1987). In the tropics of the Pacific and Atlantic oceans seasonal variations of dynamic height exceed 10.0 dynamic-cm. In the midlatitudes of the southern hemisphere seasonal variations of dynamic height exceed 7.5 dynamic-cm.

Fig. C2 shows percent variance contributed by the first Fourier harmonic to the climatological annual cycle of dynamic height. In this figure light shading indicates

areas where percent variance contributed by the first Fourier harmonic is less than 30%. In most of the northern hemisphere contribution of the first harmonic exceeds sixty percent. This is not the case for the southern hemisphere which reflects the lack of data with which we can define the climatological annual cycle in this hemisphere.

Fig. C3 shows the phase (in months) of the first Fourier harmonic of the climatological annual cycle of dynamic height. Phase is computed using formula (13). In midlatitudes maximum dynamic height occurs during Sep-Oct in the northern hemisphere and during May-July in the southern hemisphere. This pattern simply reflects the dominant role that solar heating plays in forcing the annual cycle of sea level in these regions (Gill and Niiler, 1973).

Cheney *et al.* (1994), Nerem *et al. (1994),* Chao and Fu (1995) presented amplitude and phase of the annual and semiannual variations of global sea level derived from TOPEX/POSEIDON altimeter data. Comparison of Figs. C1, C3, and C8 of this work with Fig. 6 of Cheney *et al.* (1994), Plate 3 of Nerem et al. (1994) and Fig. 2 of Chao and Fu (1995) shows good general agreement between the hydrography derived dynamic height and the altimetry derived sea level. Note, that isolines of the hydrography derived signal (this work) exhibit more noise in the southern hemisphere than in the northern hemisphere, which is associated with uneven distribution of hydrographic data between hemispheres. For the altimetry derived signal (Cheney *et al.*, 1994; Nerem *et al.,* 1994; Chao and Fu, 1995) this is not the case. Good general agreement of the hydrography derived and the altimetry derived signals in the northern hemisphere corroborates the altimetry derived signal as a whole and hence allows one to put more weight on the altimetry derived signal in the southern hemisphere where hydrographic data are sparse.

5.2 Global and basin zonal averages

In this section we describe zonal averages for the world ocean and individual ocean basins of the quantities presented in Section 4. This represents a succinct way to compare the different ocean distributions of dynamic height.

Fig. C4 shows zonally averaged annual mean dynamic height. The most striking feature is the observation that the Atlantic Ocean is lower than the Pacific and Indian Oceans at nearly all latitudes, and by more than 40 dynamic-cm in the 20^{0}S-30^{0}N latitude belt. Differences in dynamic height between the Atlantic and Pacific Oceans were described by Reid (1961) who noted a 40 dynamic-cm difference between these oceans. In addition he noted that in the 20-40 degree latitude belt, the North Pacific is approximately 10-20 dynamic-cm higher than the South Pacific - a result we confirm. However, in the Atlantic Ocean he found a similar result, whereas we find no such difference.

Zonal averages of the amplitude of first Fourier harmonic, of the percent variance of climatological annual cycle accounted for by this harmonic, and of the phase of first Fourier harmonic are presented in Figs. C5-C7. Zonal averages of the amplitude of first harmonic range from 1 to 8 dynamic-cm with the largest amplitude occurring in the 30-40 degree latitude belt of the Atlantic and Pacific Oceans and the South Indian Ocean, and at about 12^{0}N in the North Indian Ocean. As seen in Figs. C1-C3, the southern hemisphere analyses are relatively noisy compared to the northern hemisphere analyses. This is clearly illustrated by the zonally averaged distributions of percent variance (Fig. C7). The percent variance accounted for by the first harmonic generally exceeds 60 percent in midlatitudes of the northern hemisphere as compared to 30-40 percent in the southern hemisphere. This is simply due to the relative paucity of data in the southern as compared to northern hemisphere. In the tropical Pacific distinct relative maxima occur at 7^{0}S, 7^{0}N, and 13^{0}N, whereas in the tropical Atlantic a maximum occurs at about 8^{0}S and a broad maximum occurs centered on the Equator. In the North Pacific and North. Atlantic oceans the maximum in dynamic height is clearly seen to occur during September, whereas in the southern hemisphere extratropics of these basins the maximum occurs during April-July.

Contribution of the second Fourier harmonic to the climatological annual cycle of dynamic height is most significant in the tropical oceans. Figs. C8-C9 show amplitude of and percent variance contributed by the second harmonic. In the equatorial and tropical Indian Ocean the amplitude of the second harmonic exceeds 7.5 dynamic-cm in some locations and the percent variance contribution exceeds sixty percent. Figs. C10-C12 show zonal averages of the amplitude of the second harmonic, percent variance of the climatological annual cycle accounted for by this harmonic, and phase of this harmonic. We have presented these distributions for all basins because the second harmonic is of importance in the tropics of all three basins and represents a major

signal in the tropical Indian Ocean. For example in the 8^0S-5^0N latitude belt of this ocean the amplitude of this harmonic is approximately 4 dynamic-cm, which accounts for about 38 percent of the variance of the annual cycle.

5.3 Comparison of climatological hemispheric annual cycles with TOPEX altimeter estimates

Fig. D1 shows the seasonal cycle of hemispherically averaged sea level for forty-one months of TOPEX altimeter data plotted along with the climatological seasonal cycle of steric sea level computed from the fields described in this atlas. On a hemispheric scale, the seasonal cycle of sea level and steric sea level are clearly determined by the annual temperature cycle of these regions. The agreement between the two data sets is better for the northern hemisphere than the southern hemisphere. We attribute this to better data coverage of the northern hemisphere. If we were to compare the seasonal cycles for smaller regions than we would expect there to be greater differences between the two data sets because of the effects of interannual variability.

6. SUMMARY

We have presented climatological monthly mean fields of dynamic height 0-1000 m along with differences between monthly mean and annual mean fields.

A Fourier analysis of the climatological annual cycle of dynamic height 0-1000 m indicates that the first harmonic is the dominant contributor to the annual cycle for most of the world ocean. The second harmonic plays an important role in the tropical Indian Ocean and in some portions of the tropical Atlantic and Pacific Oceans.

REFERENCES

Anderson, D.L.T., and R.A. Corry, 1985: Ocean response to low-frequency wind forcing with application to the seasonal variation in the Florida Straits-Gulf Stream transport. *Prog. Oceanogr.*, 14, 7-40.

Barnett, T.P., 1983: Recent changes in sea level and their possible causes. *Climatic Change*, 5, 15-38.

Cartwright, M., 1990: Fourier Methods for Mathematicians, Scientists and Engineers. Ellis Horwood Press, New York, 326 pp.

Chatfield, C., 1989: The analysis of time series. Chapman and Hall, London, 241 pp.

Chao, Yi., and L-L. Fu, 1995: A comparison between the TOPEX/POSEIDON data and a global ocean general circulation model during 1992-1993. *J. Geophys. Res.*, 100, 24,965-24,976.

Cheney, R.E., B.C. Douglas, D.C. MacAdoo, and D.T. Sandwell, 1986: Geodetic and oceanographic applications of satellite altimetry. In *Space Geodesy and Geodynamics*, Eds. A.J. Anderson and A. Cazenave, Academic Press, New York, 377-405.

_____, L. Miller, R. Agreen, N Doyle, and J. Lillibridge, 1994: TOPEX/POSEIDON: The 2-cm solution. *J. Geophys. Res.*, 99, 24,555-24,563.

Douglas, B.C., 1991: Global sea level rise. *J. Geophys. Res.*, 96, 6981-6992.

_____, B.C., 1992: Global sea level acceleration. *J. Geophys. Res.*, 97, 12,699-12,706.

Fofonoff, N.P., and R.C. Millard Jr., 1983: Algorithms for computation of fundamental properties of seawater. *UNESCO Technical Paper in Marine Science* 44.

Fu, L-L, J. Vazquez, and M.E. Parke, 1987: Seasonal variability of the Gulf Stream from satellite altimetry. *J. Geophys. Res.*, 92, 749-754.

Gill, A.E., and P.P., Niiler, 1973: The theory of the seasonal variability in the ocean. Deep-Sea Res., 20, 141-177.

Greatbatch, R., and A. Goulding, 1989: Seasonal variations in a linear barotropic model of the North Atlantic driven by the Hellerman and Rosenstein wind stress field. *J. Phys. Oceanogr.* 19, 572-595.

Gornitz, V., 1995: Monitoring sea level changes. *Climatic Change*, 31, 515-544.

Halkin, D., and T. Rossby 1985: The structure and transport of the Gulf Stream at 73W. *J. Phys. Oceanogr.*, 15, 1439-1452.

Hicks, S.D., Debaugh, H.A., and Hickman, L.E., 1983: Sea level variations for the United States 1855-1980. N*ational Ocean Service Report*, Tides and Water Levels Branch. Rockville, Md., 170 pp.

Lambeck, K., *1980: The earth's variable rotation: Geophysical causes and consequences*, 449 pp., Cambridge University Press, Cambridge.

Levitus, S., 1982: Climatological Atlas of the World Ocean. *NOAA Professional Paper* 13., U.S. Government Printing

Office, Washington, D.C., 1982, 173 pp.

_____, 1987: Rate of change of heat storage of the world ocean. *J. Phys. Oceanogr.*, 17, 518-528.

_____, R. Gelfeld, T. Boyer, and D. Johnson, 1994a: Results of the NODC and IOC Oceanographic Data Archeology and Rescue Projects: Report 1, NOAA, Washington, D.C., 73 pp.

_____, T. Boyer, 1994b: World Ocean Atlas 1994, Vol. 4: Temperature. *NOAA Atlas NESDIS 4*, 117 pp., U.S. Gov. Printing Office, Washington, D.C.

_____ , 1994c: R. Burgett, T. Boyer, World Ocean Atlas 1994, Vol. 3: Salinity. *NOAA Atlas NESDIS 3*, 99 pp., U.S. Gov. Printing Office, Washington, D.C.

Lisitzin, E., *1974: Sea Level Changes*, Elsevier, New York, 286 pp.

Merle, J., 1980: Seasonal heat budget in the equatorial Atlantic Ocean. *J. Phys. Oceanogr.*, 10, 464-469.

Montgomery, R.B., 1938: Fluctuations in monthly sea level on eastern U.S. coast as related to dynamics of western North Atlantic. *J. Mar. Res.*, 1, 165-185.

Munk, W.H., and R. Revelle, 1952: Sea level and the rotation of the Earth. *Amer. J. Science,* 250, 829-833.

_____, and G.J.F. MacDonald, 1960: *The rotation of the earth: A geophysical discussion.*, Cambridge University Press., 313 pp.

Nerem, R. S., Schrama E.J., Koblinsky C.J., and B.D. Beckley, 1994: A preliminary evaluation of ocean topography from the TOPEX/POSEIDON mission. *J. Geophys. Res.*, 99, 24,565-24,583.

Neumann, G., and W.J. Pierson, 1966: *Principles of Physical Oceanography*, 545 pp., Prentice Hall. Englewood Cliffs, N.J., US.

Patullo, J.G., Munk, W.H., Revelle, R., and E. Strong, 1955: The seasonal oscillation of sea level. *J. Mar. Res*, 14, 88-155.

Philander, S.G.H., 1978: Forced oceanic waves, *Rev. Geophys. Space Phys.*, 16, 15-46.

Pugh, D.T., 1987: *Tides, Surges, and Mean Sea-Level: A Handbook for Engineers and Scientists*. Wiley and Sons, New York, 472 pp.

Reid, J.L., 1961: On the temperature, salinity, and density differences between the Atlantic and Pacific Oceans in the upper kilometer. *Deep-Sea Res.*, 7, 265-275.

Sandstrom, J.W., 1903: Ueber die an wendung von pegelbeobachtungen zur berechnung der gerschwindigkeit der meerestrome. Svenska Hydrografisk Biologiska Kommissionens Skrifter, 1.

Stommel, H., 1964: Summary charts of the mean dynamic topography and current field at the surface of the ocean, and related functions of the mean wind stress. In: *Studies on Oceanography.* Kozo Yoshida, ed. University of Tokyo Press. Tokyo, Japan.

Woodworth, P.L., 1984: The world wide distribution of the seasonal cycle of mean sea level. *Institute of Oceanographic Sciences, Report N~190*, 94 pp., Surrey, England.

Wyrtki, K., 1971: Oceanographic Atlas of the Indian Ocean Expedition, National Science Foundation, Wash., D.C., 531 pp.

_____, K., 1975: Fluctuations of the dynamic topography in the Pacific Ocean. *J. Phys. Oceanogr.*, 5, 450-459.

_____, K., L. Magaard, and J. Hager, 1976: Eddy energy in the oceans. *J. Geophys. Res.*, 81, 2641-2646.

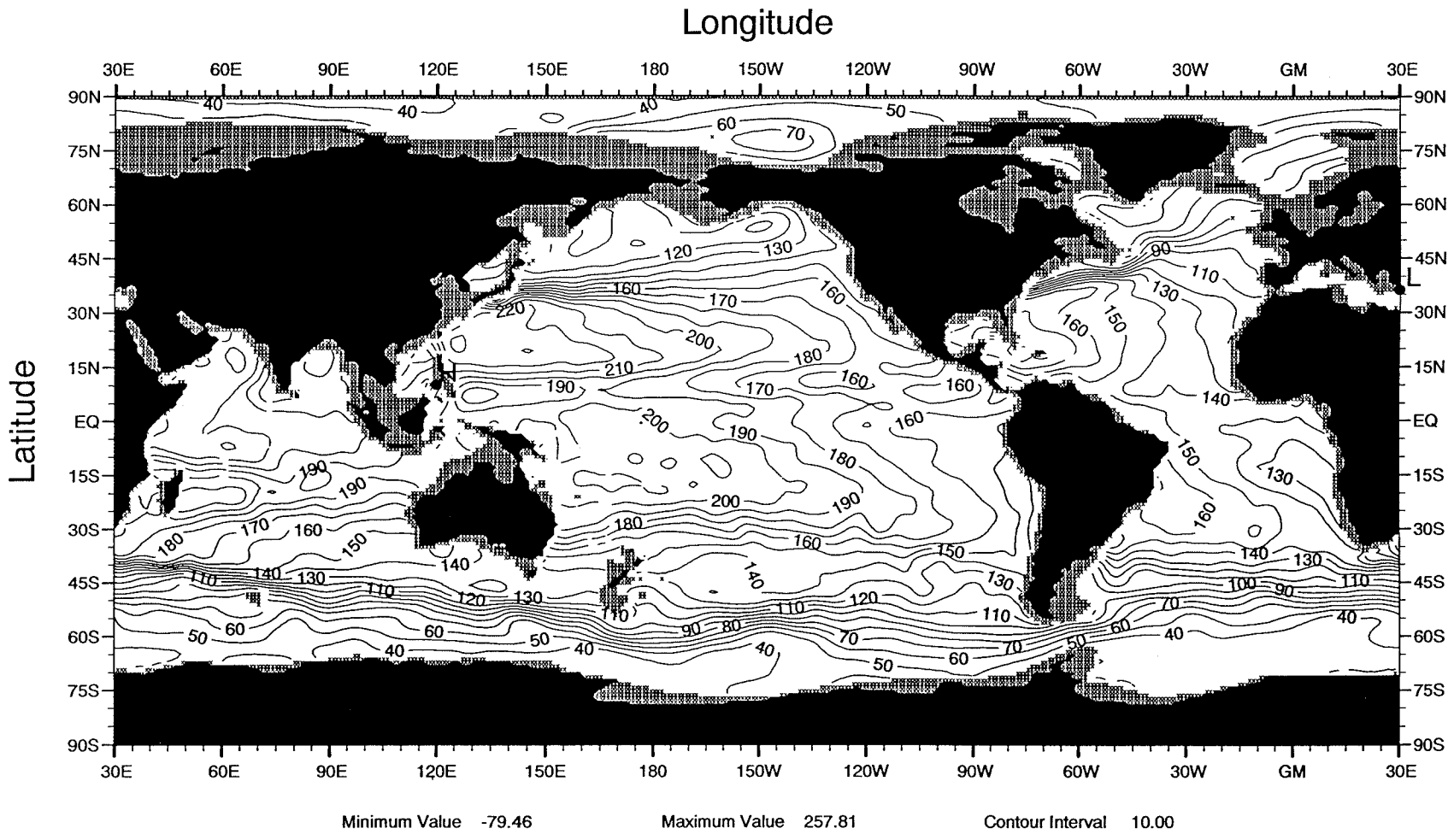

Fig. A1 January mean dynamic height (dynamic cm) 0 - 1000 m

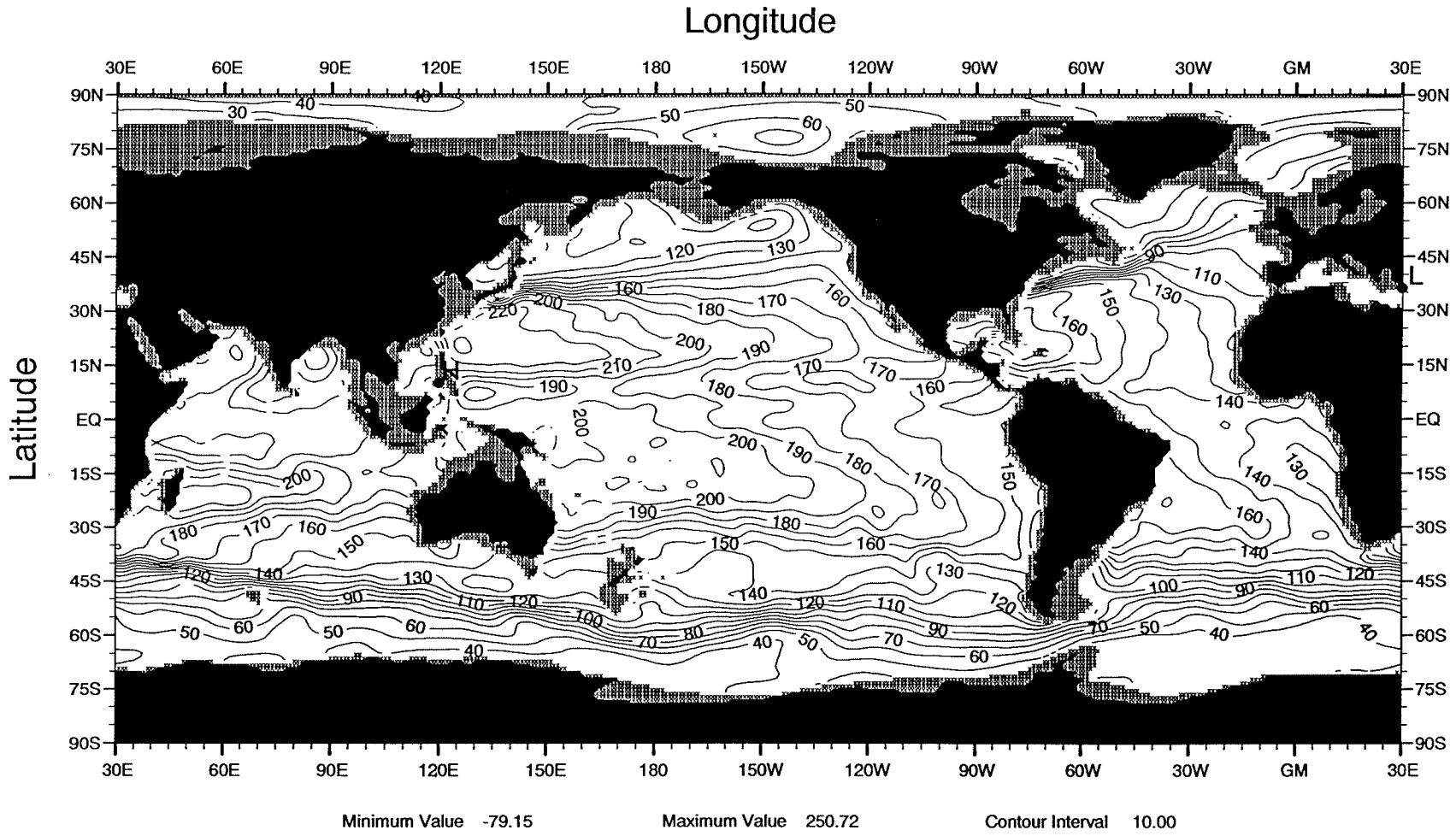

Fig. A2 February mean dynamic height (dynamic cm) 0 - 1000 m

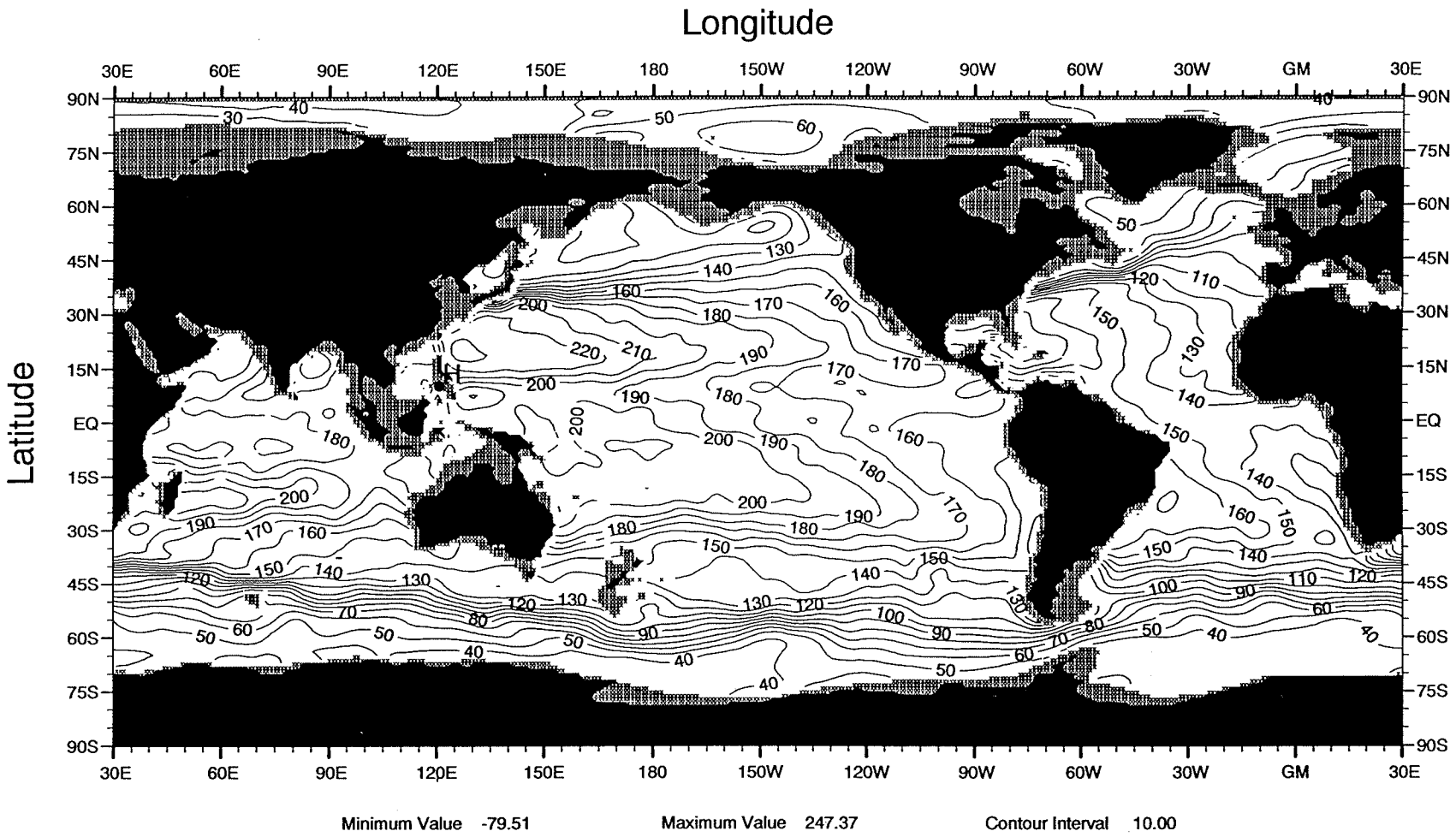

Fig. A3 March mean dynamic height (dynamic cm) 0 - 1000 m

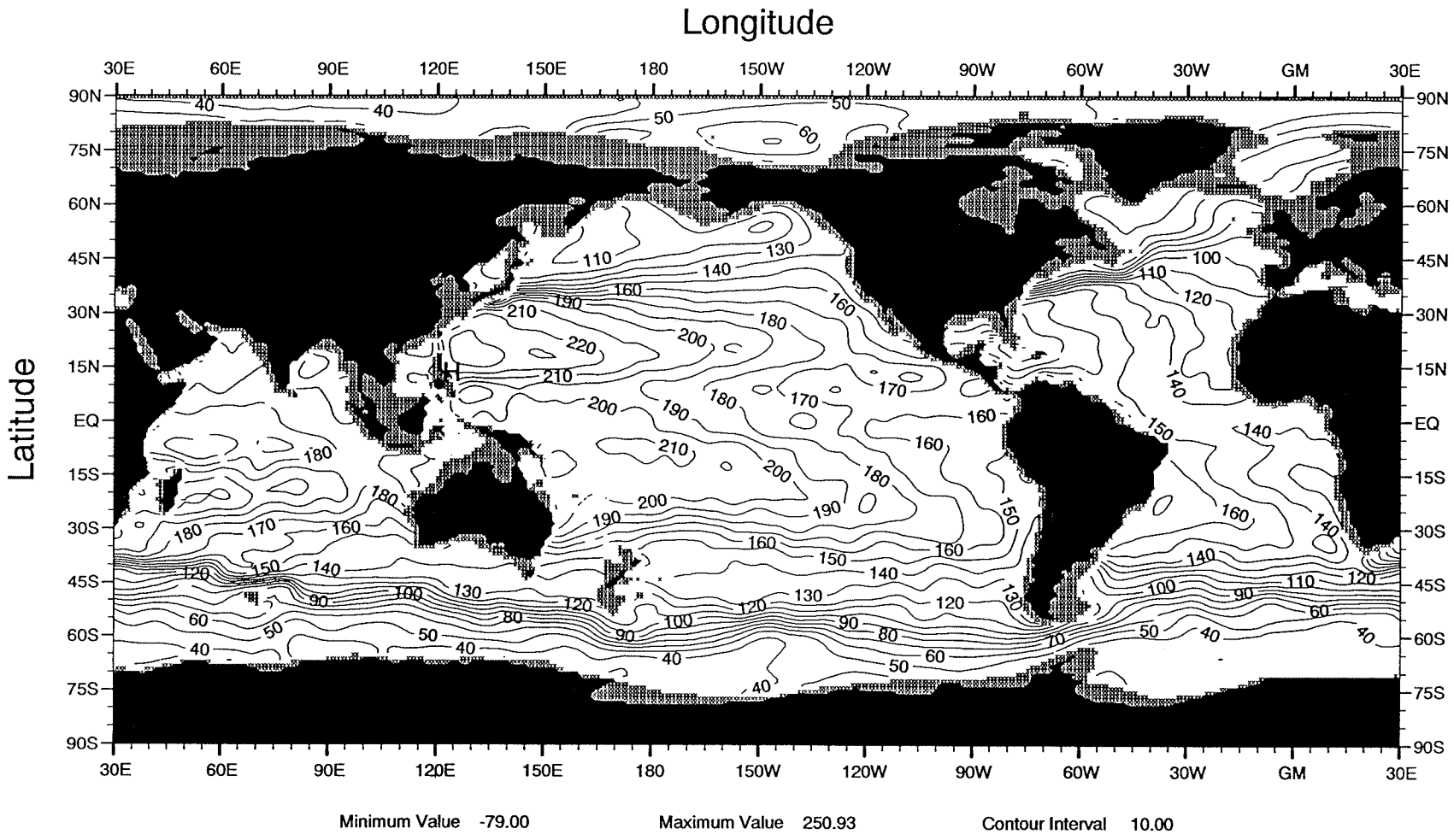

Fig. A4 April mean dynamic height (dynamic cm) 0 - 1000 m

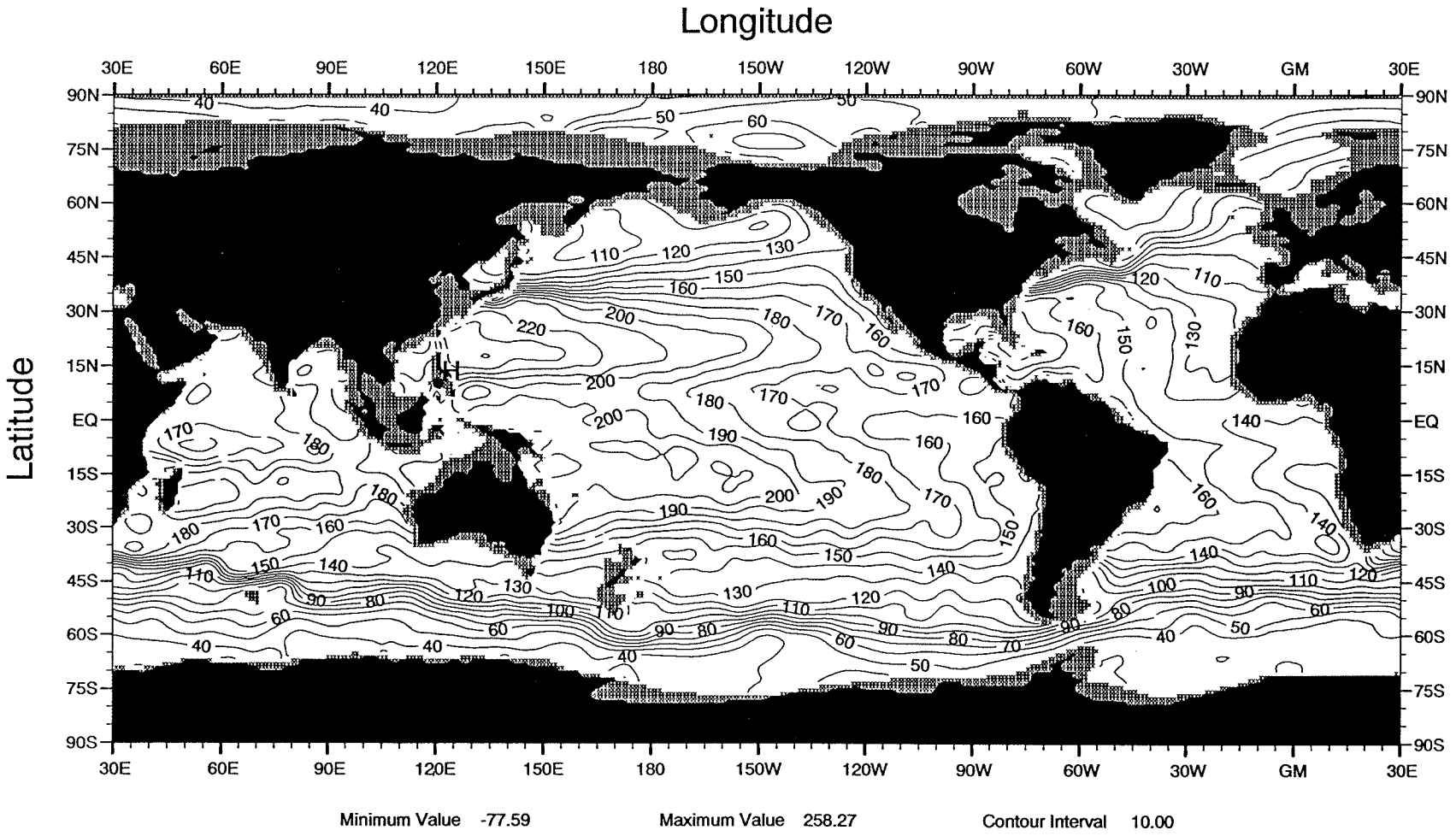

Fig. A5 May mean dynamic height (dynamic cm) 0 - 1000 m

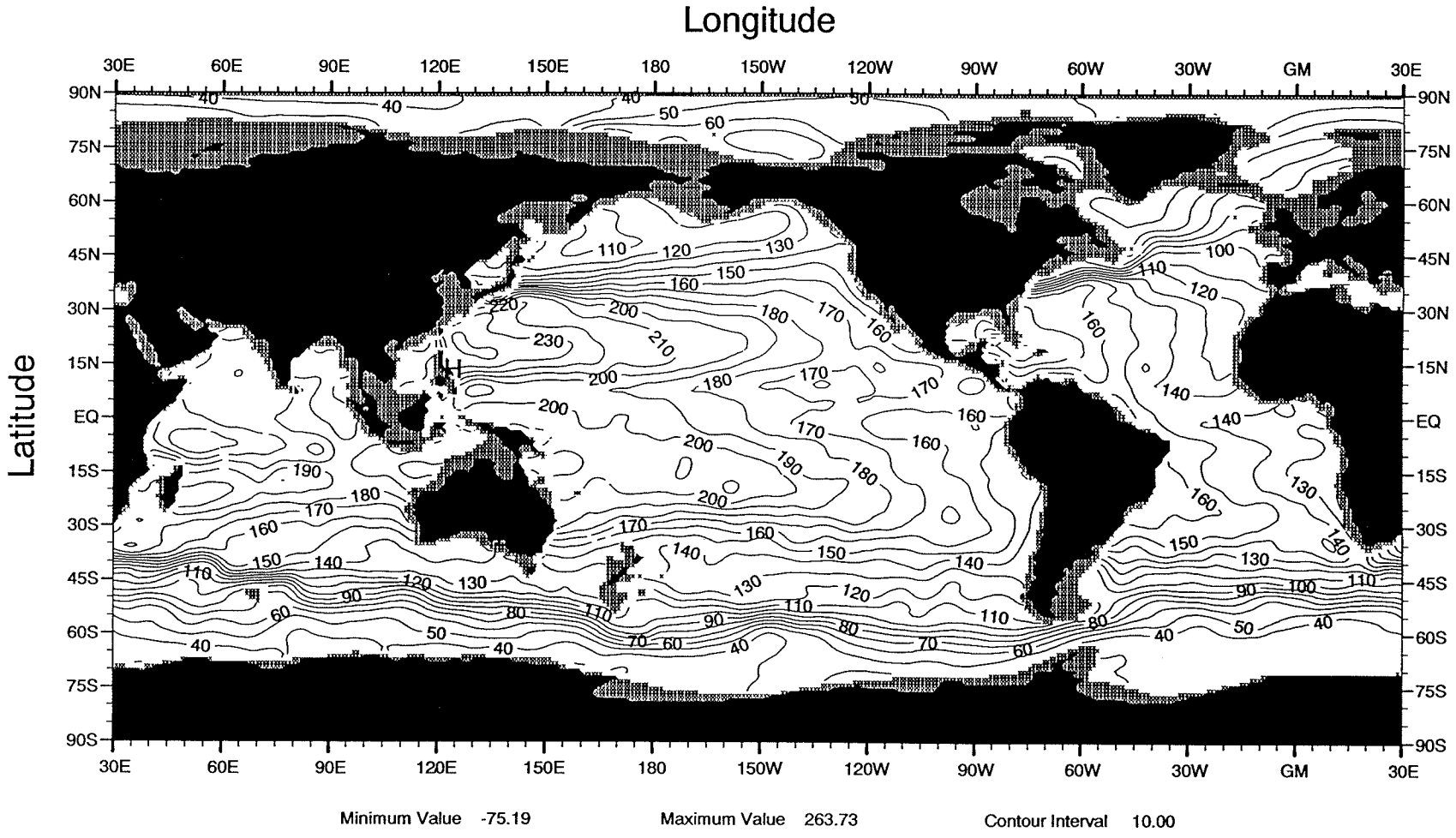

Fig. A6 June mean dynamic height (dynamic cm) 0 - 1000 m

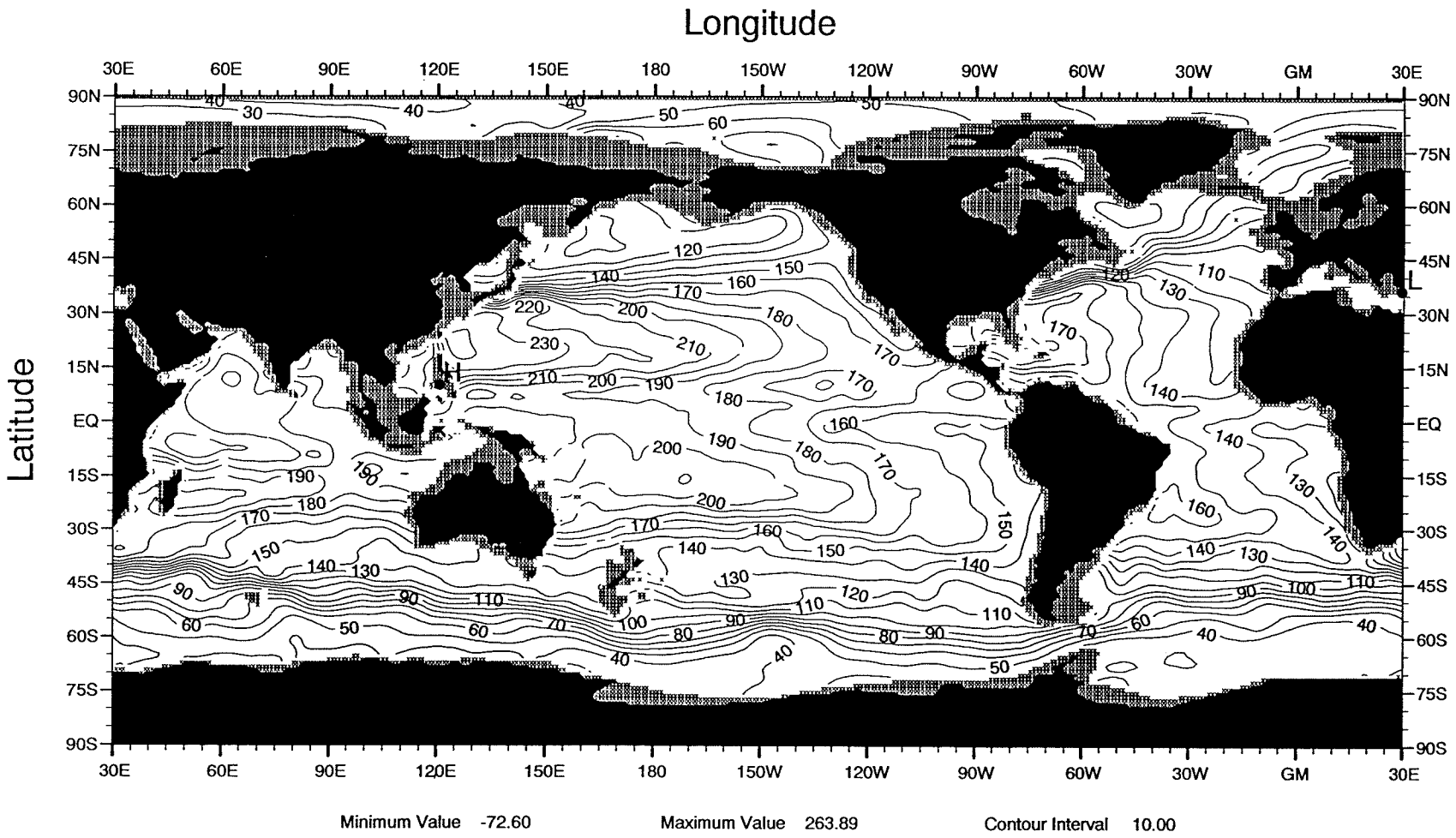

Fig. A7 July mean dynamic height (dynamic cm) 0 - 1000 m

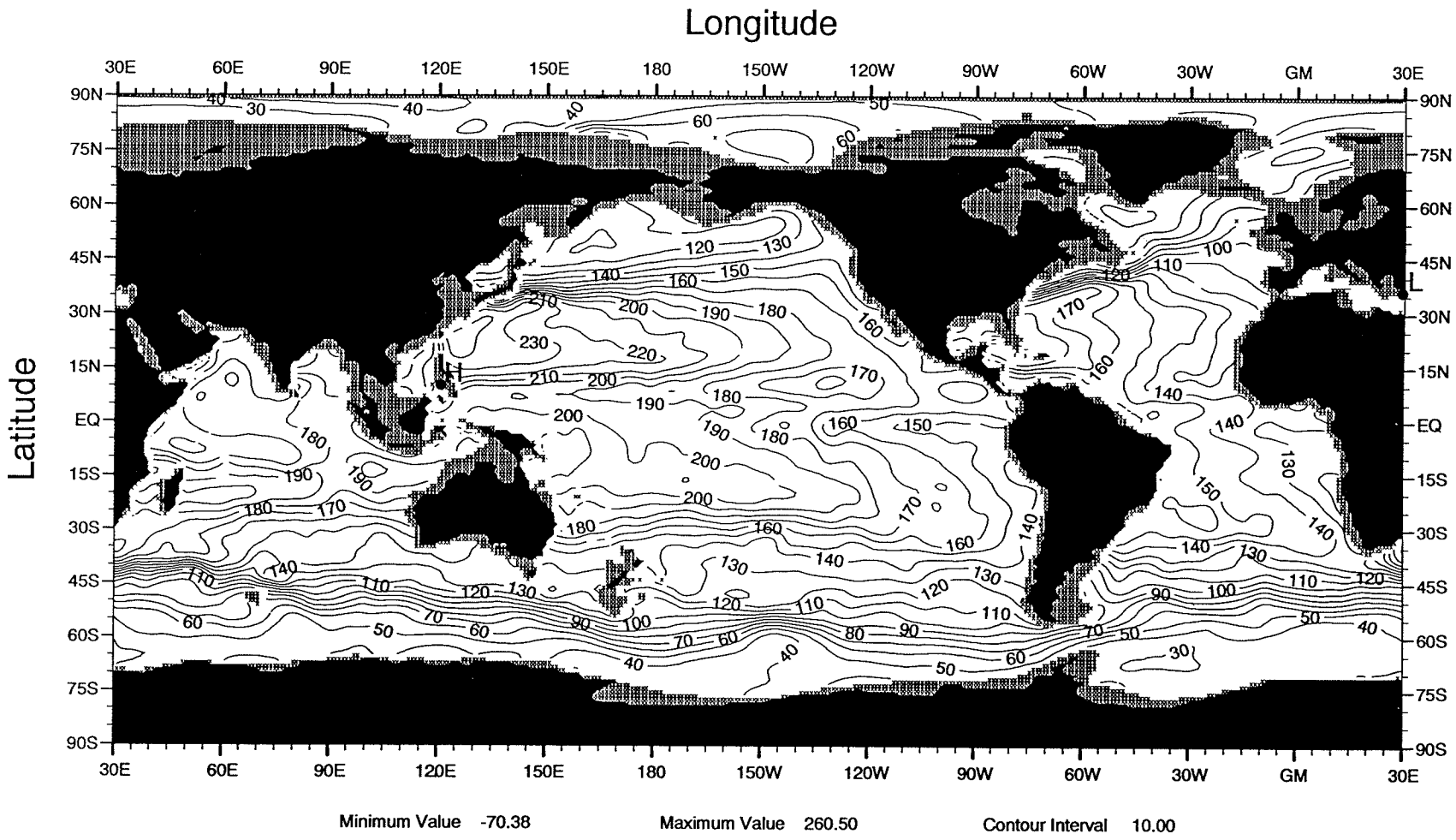

Fig. A8 August mean dynamic height (dynamic cm) 0 - 1000 m

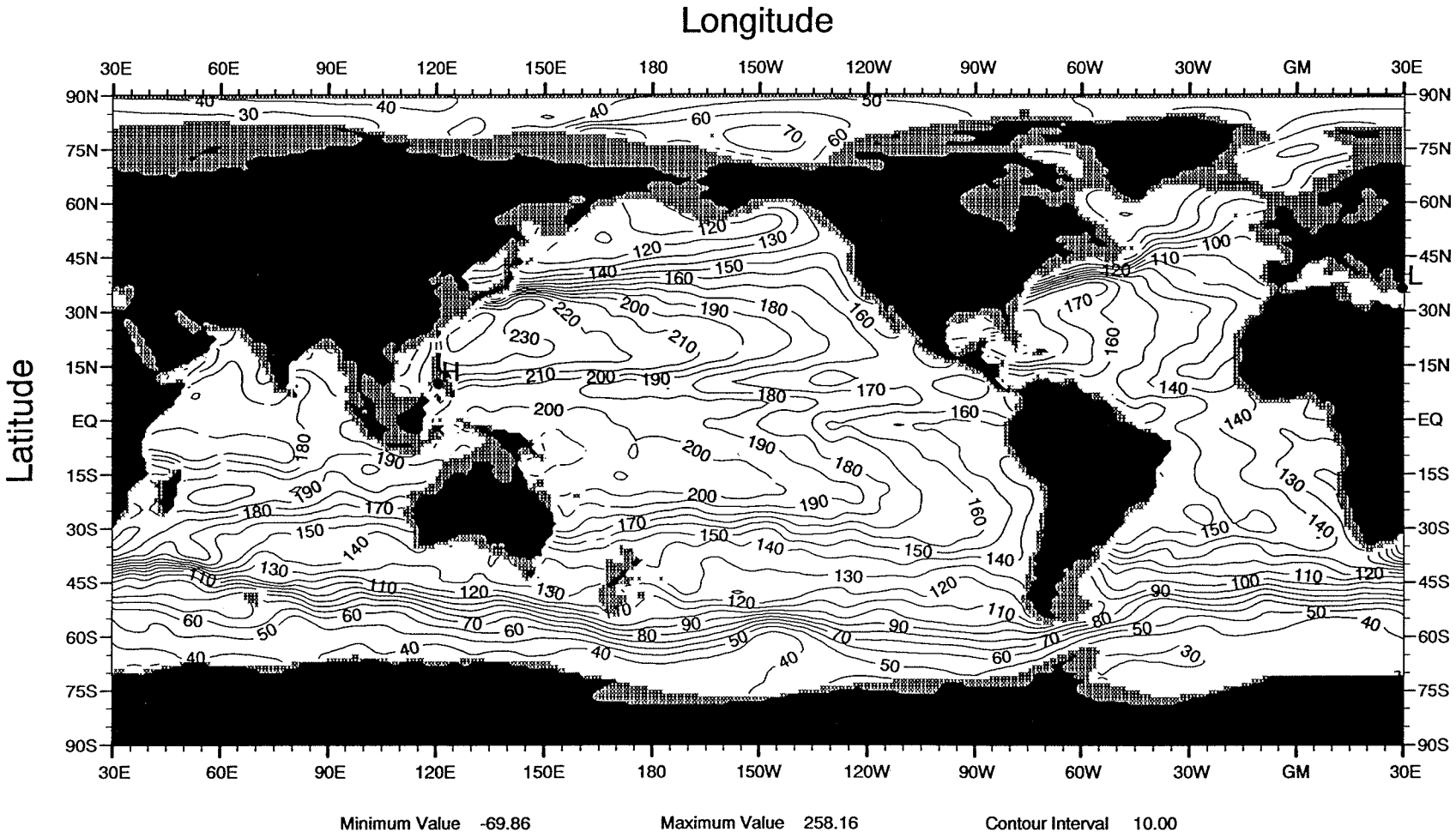

Fig. A9 September mean dynamic height (dynamic cm) 0 - 1000 m

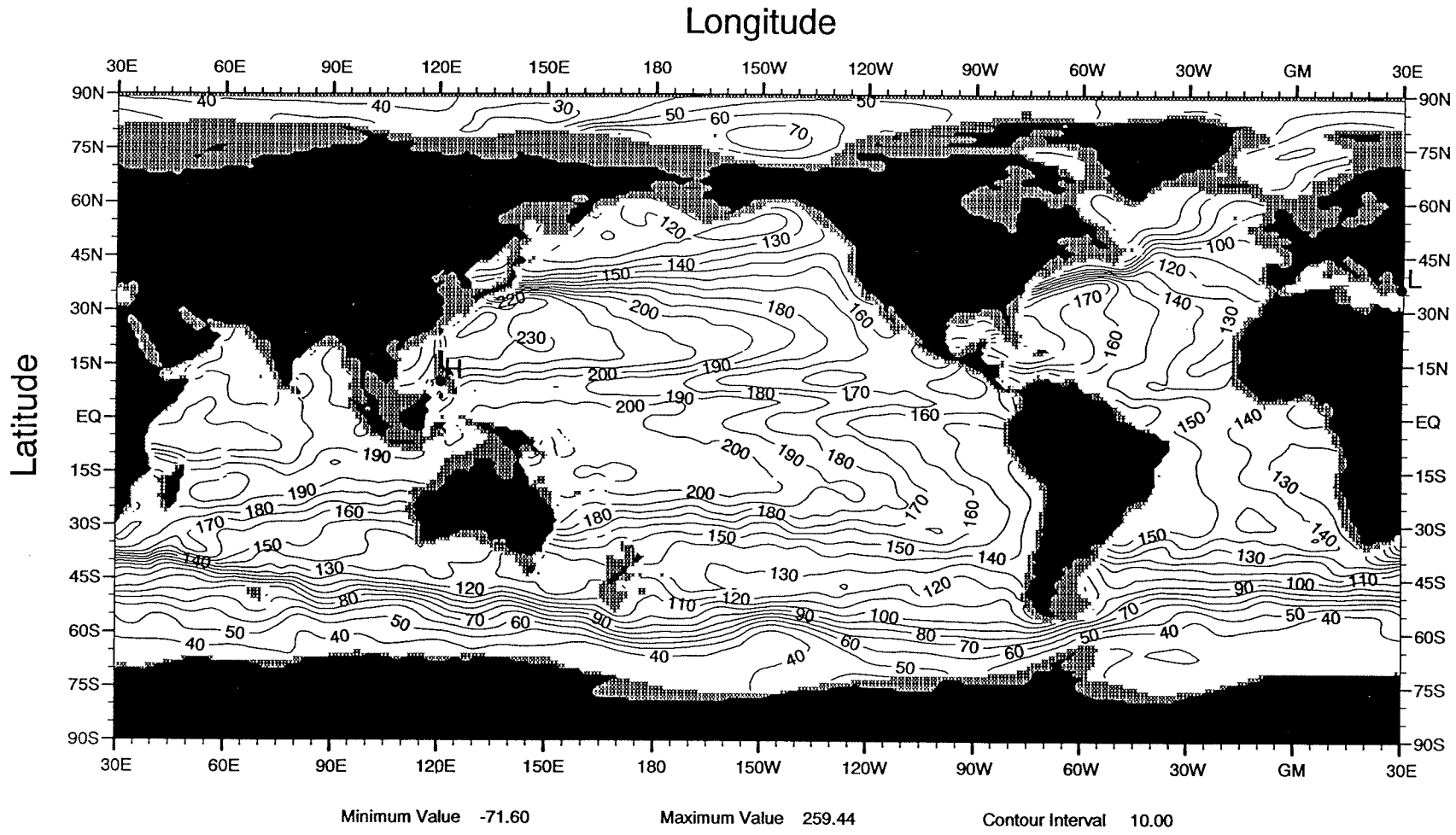

Fig. A10 October mean dynamic height (dynamic cm) 0 - 1000 m

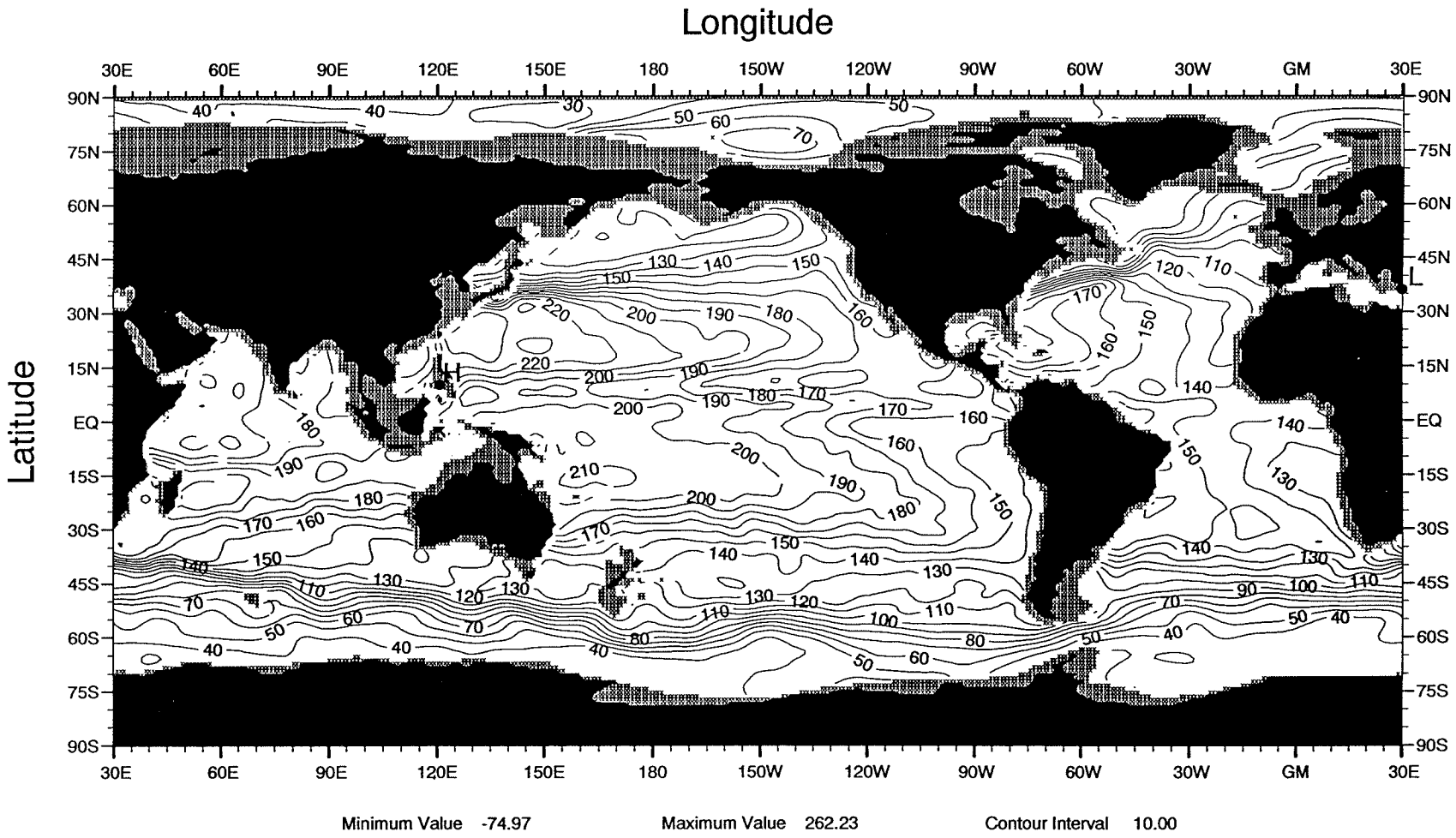

Fig. A11 November mean dynamic height (dynamic cm) 0 - 1000 m

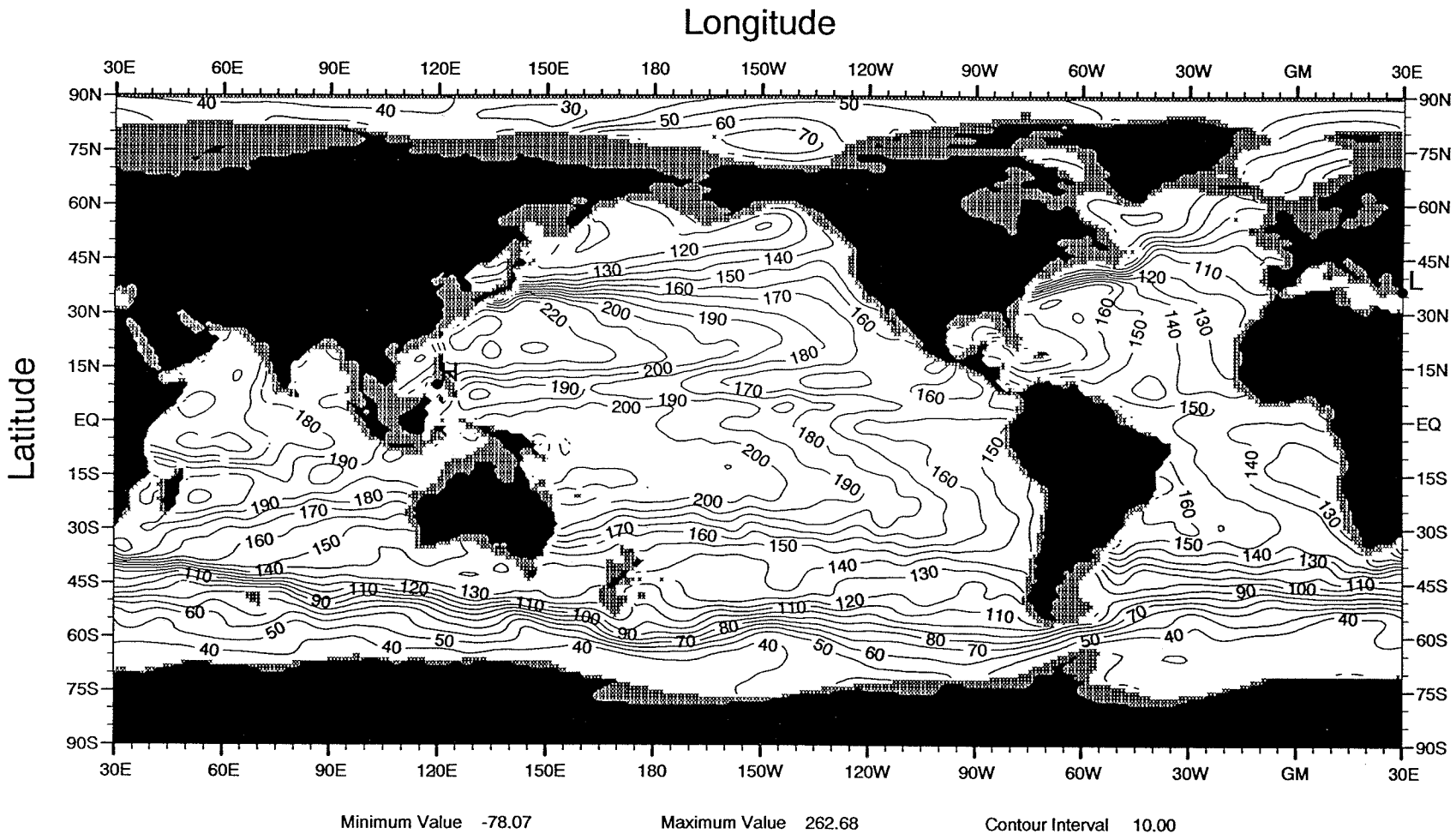

Fig. A12 December mean dynamic height (dynamic cm) 0 - 1000 m

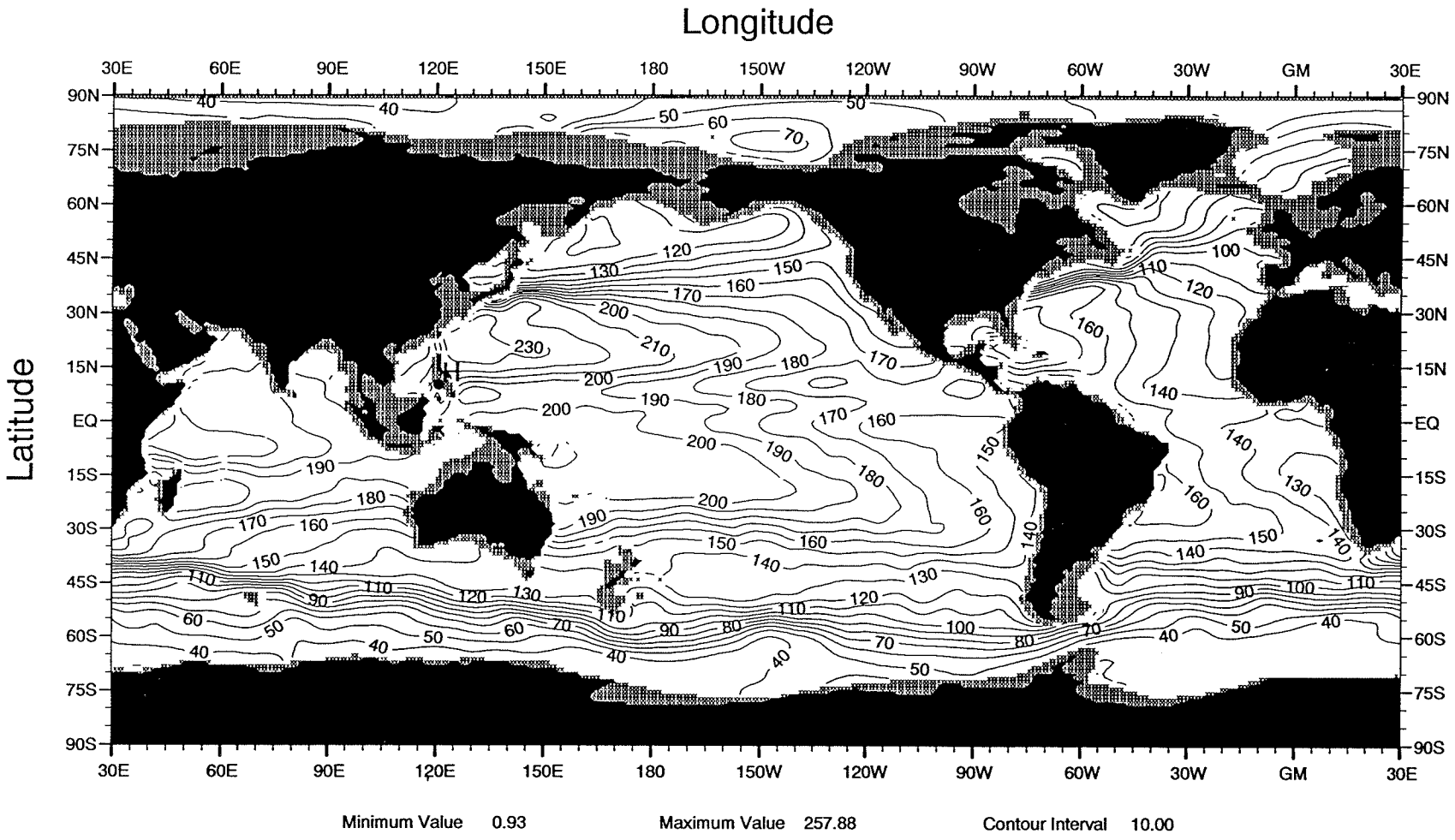

Fig. A13 Annual mean dynamic height (dynamic cm) 0 - 1000 m

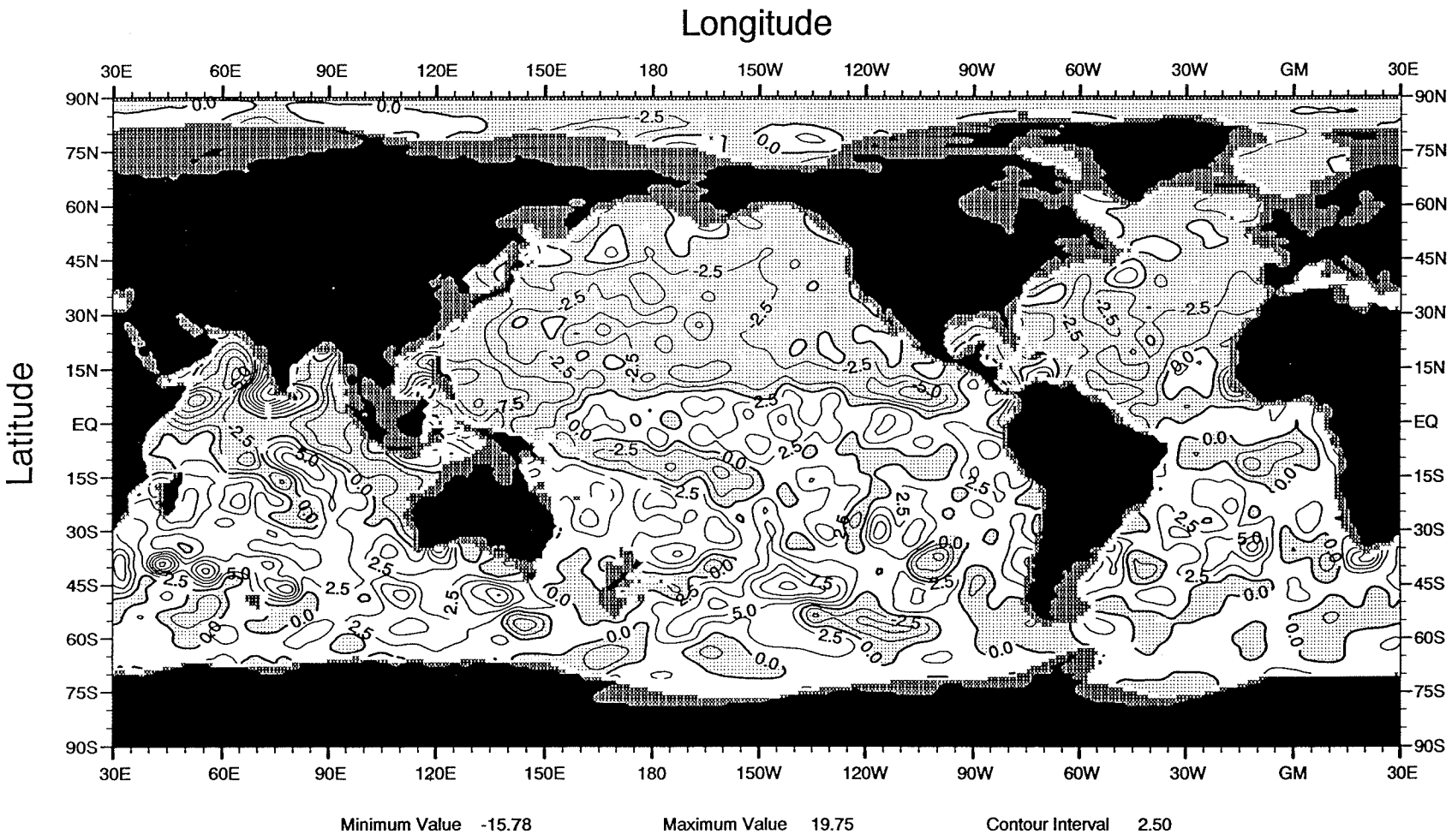

Fig. B1 January mean minus annual mean dynamic height (dynamic cm) 0 - 1000 m

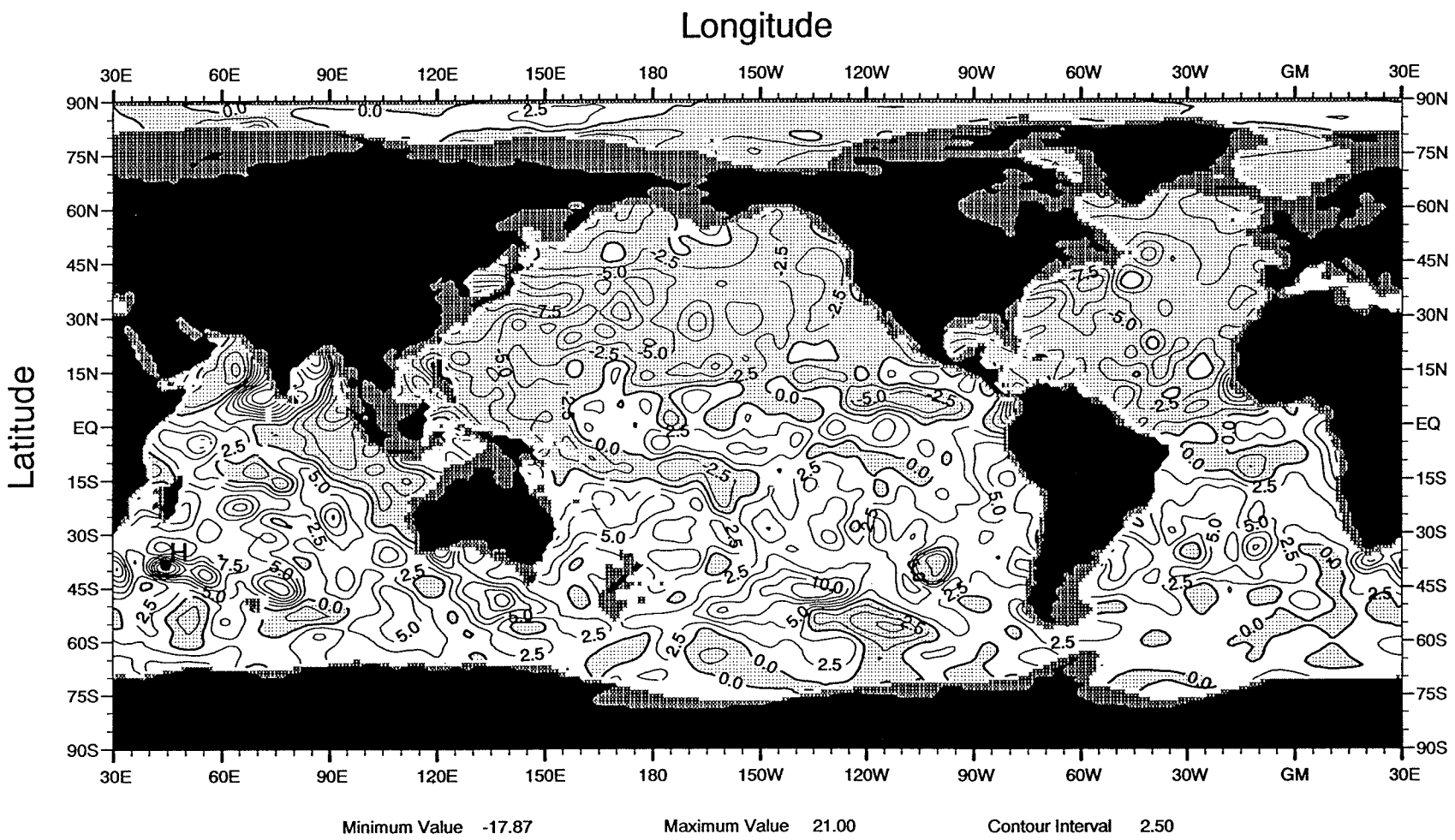

Fig. B2 February mean minus annual mean dynamic height (dynamic cm) 0 - 1000 m

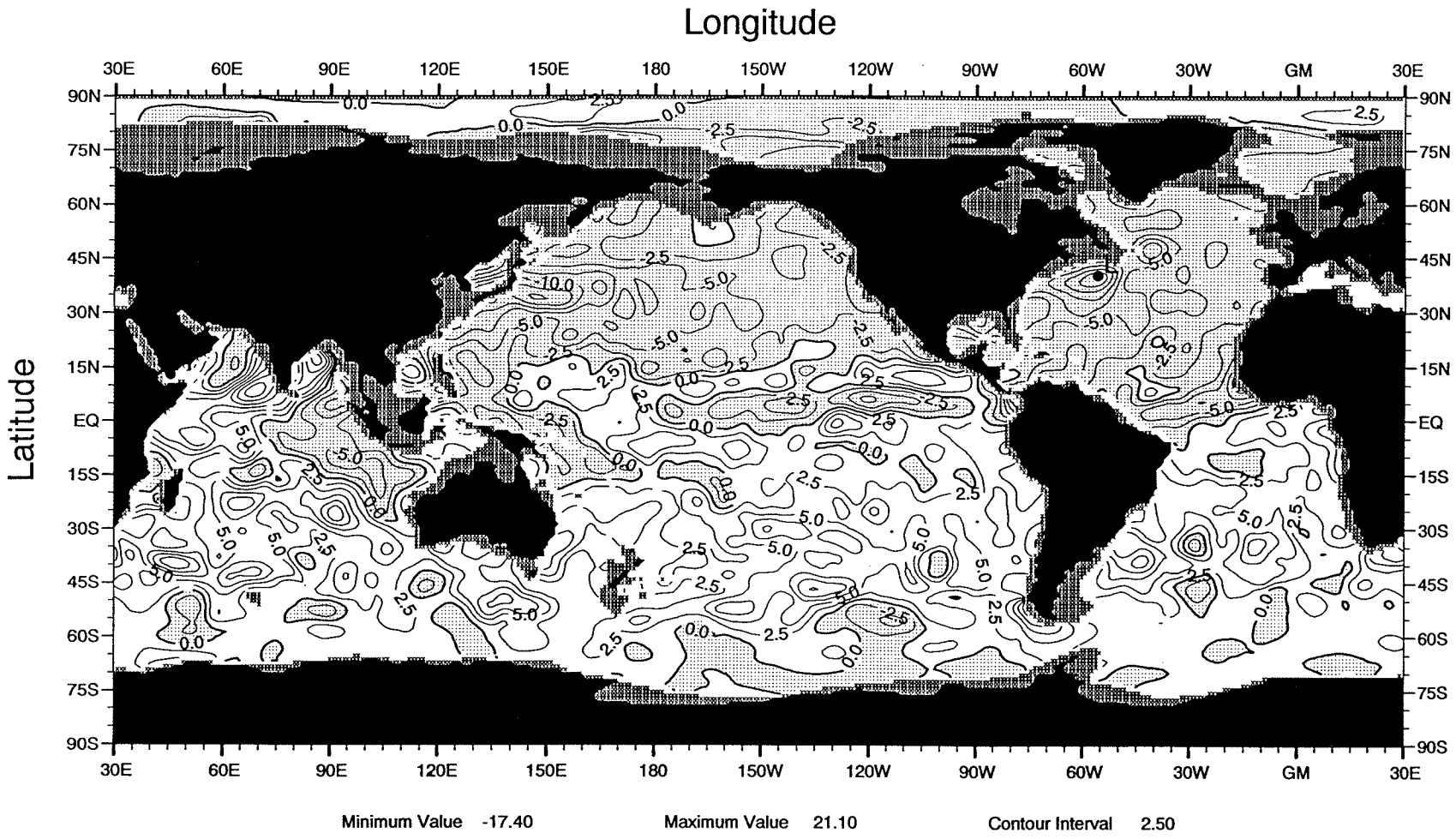

Fig. B3 March mean minus annual mean dynamic height (dynamic cm) 0 - 1000 m

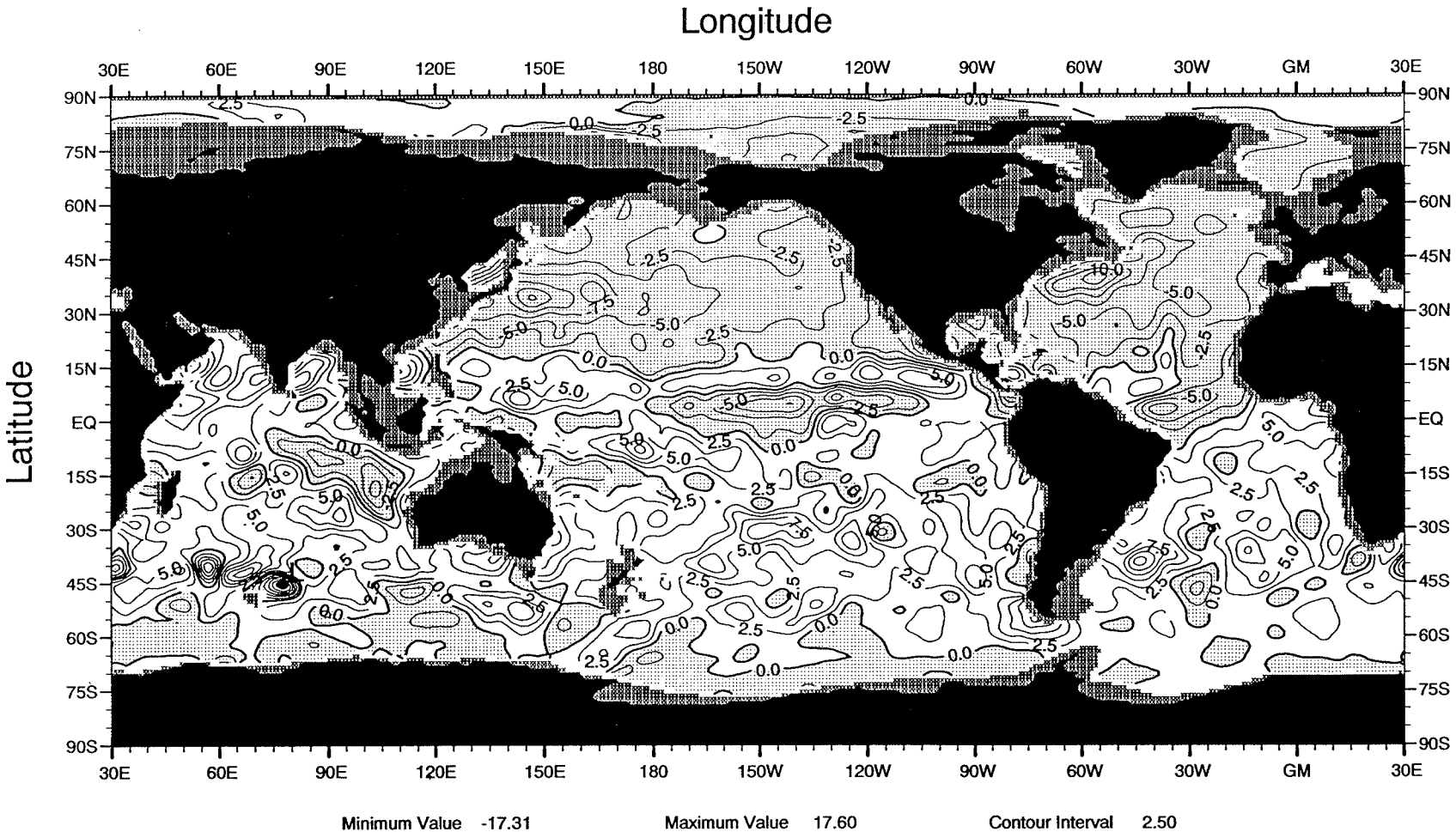

Fig. B4 April mean minus annual mean dynamic height (dynamic cm) 0 - 1000 m

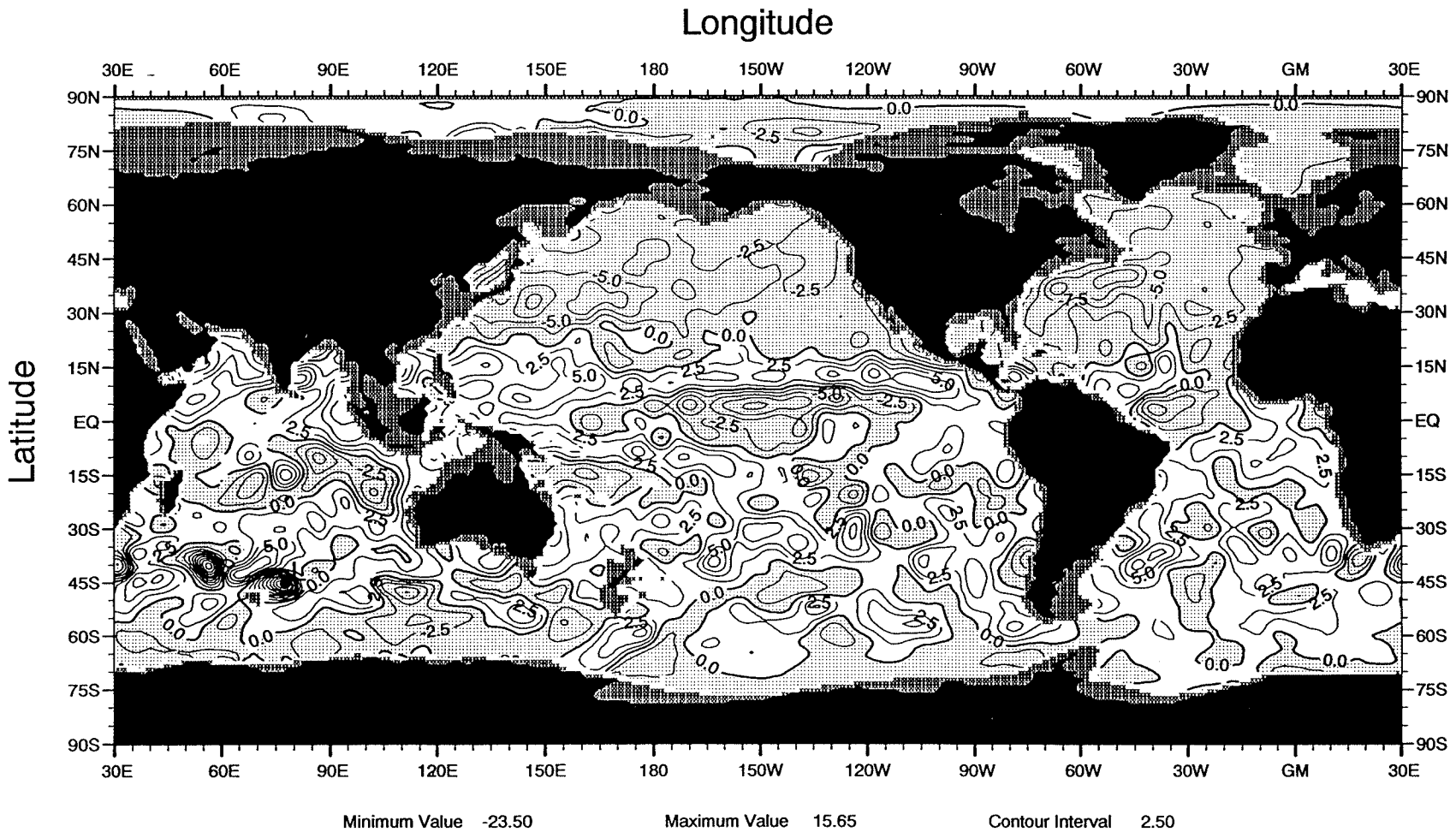

Fig. B5 May mean minus annual mean dynamic height (dynamic cm) 0 - 1000 m

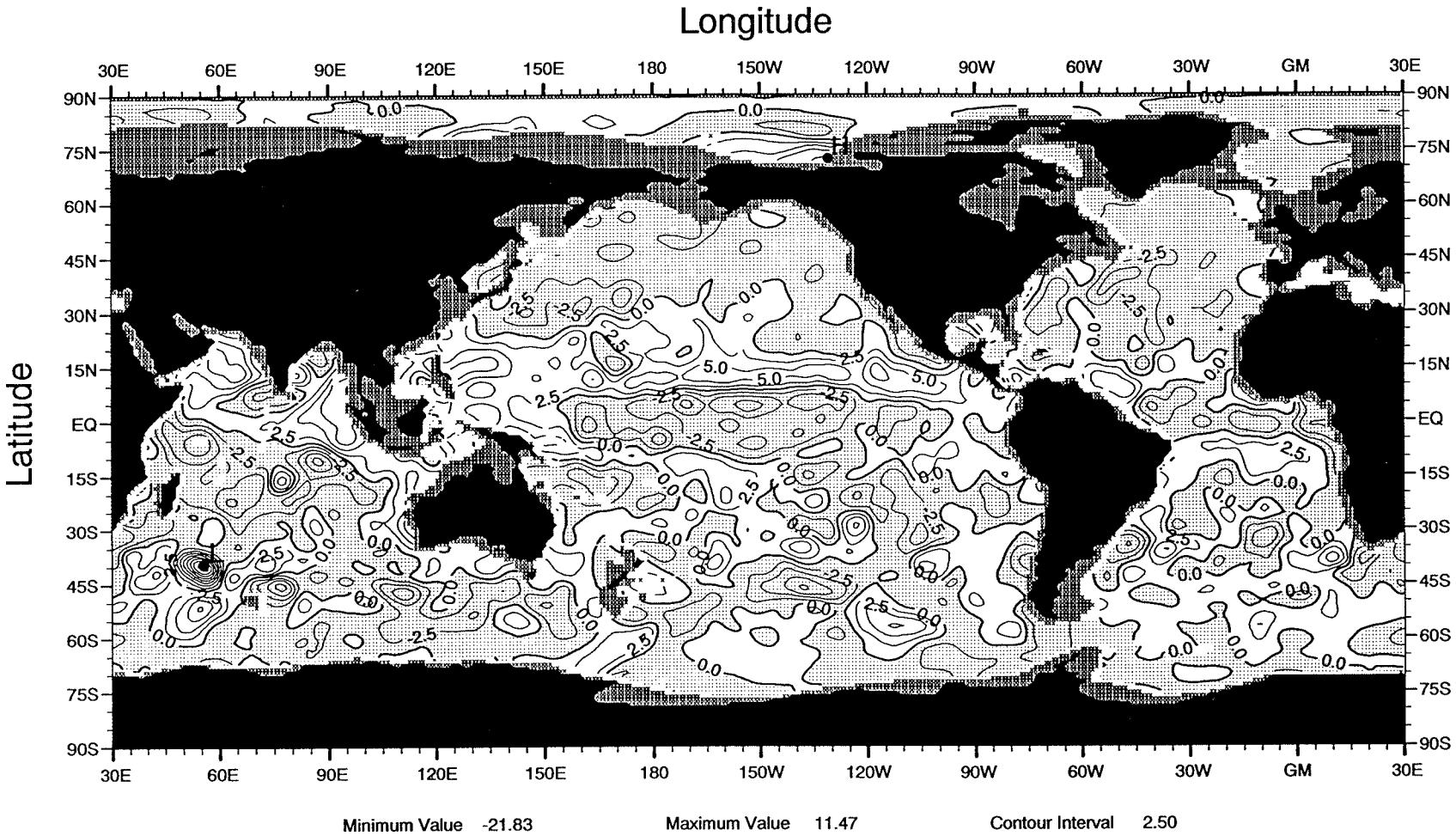

Fig. B6 June mean minus annual mean dynamic height (dynamic cm) 0 - 1000 m

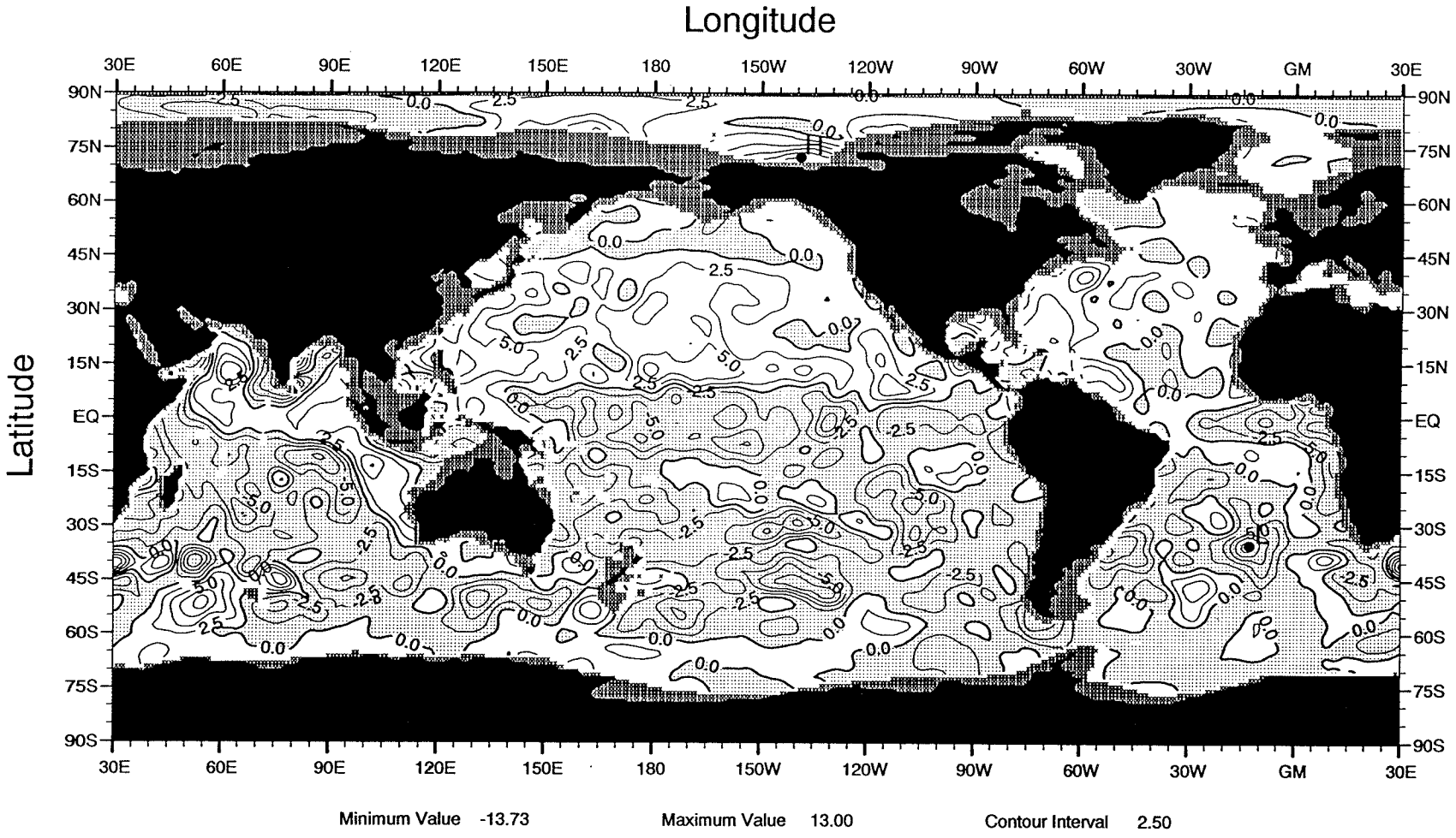

Fig. B7 July mean minus annual mean dynamic height (dynamic cm) 0 - 1000 m

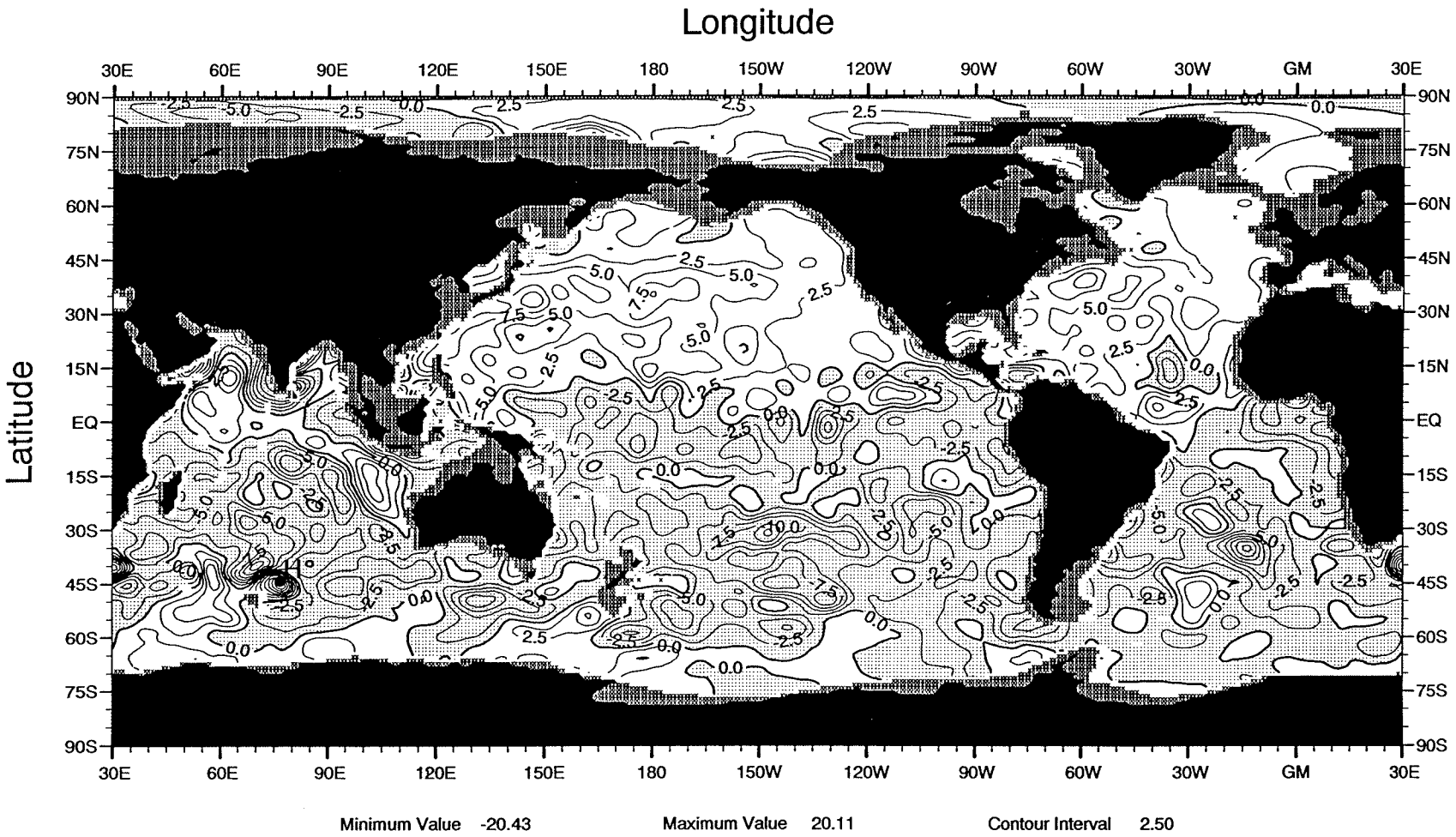

Fig. B8 August mean minus annual mean dynamic height (dynamic cm) 0 - 1000 m

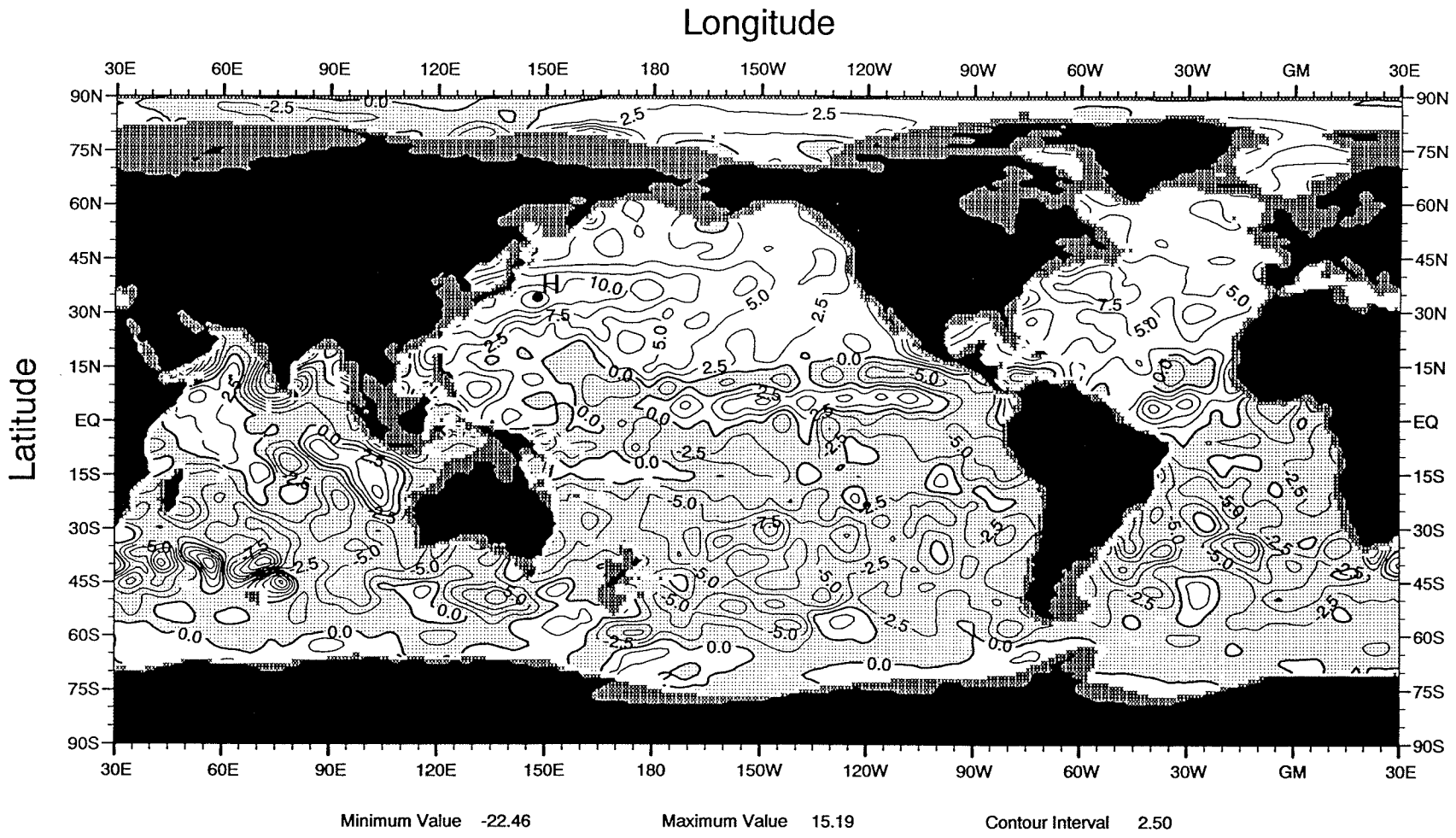

Fig. B9 September mean minus annual mean dynamic height (dynamic cm) 0 - 1000 m

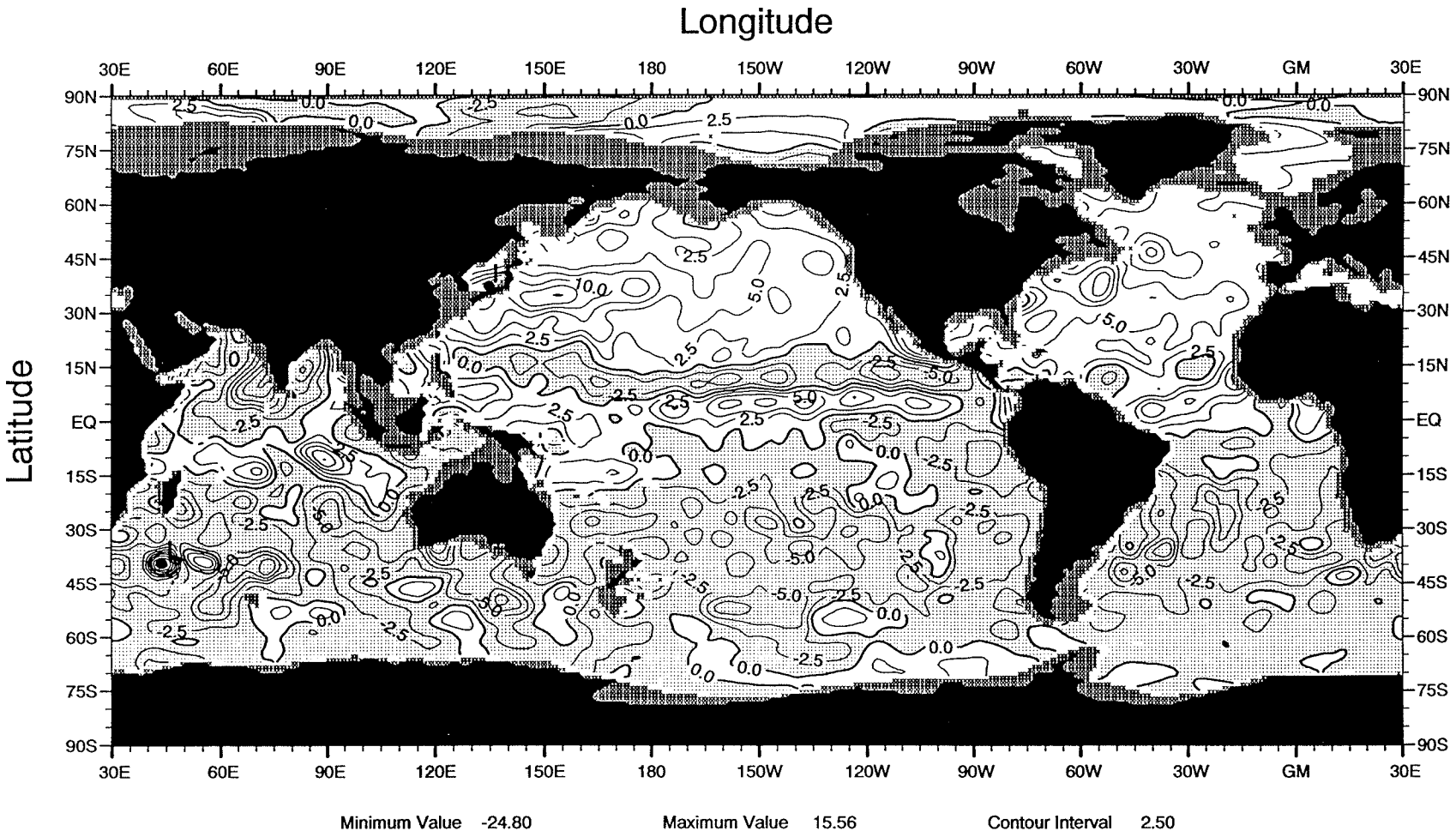

Fig. B10 October mean minus annual mean dynamic height (dynamic cm) 0 - 1000 m

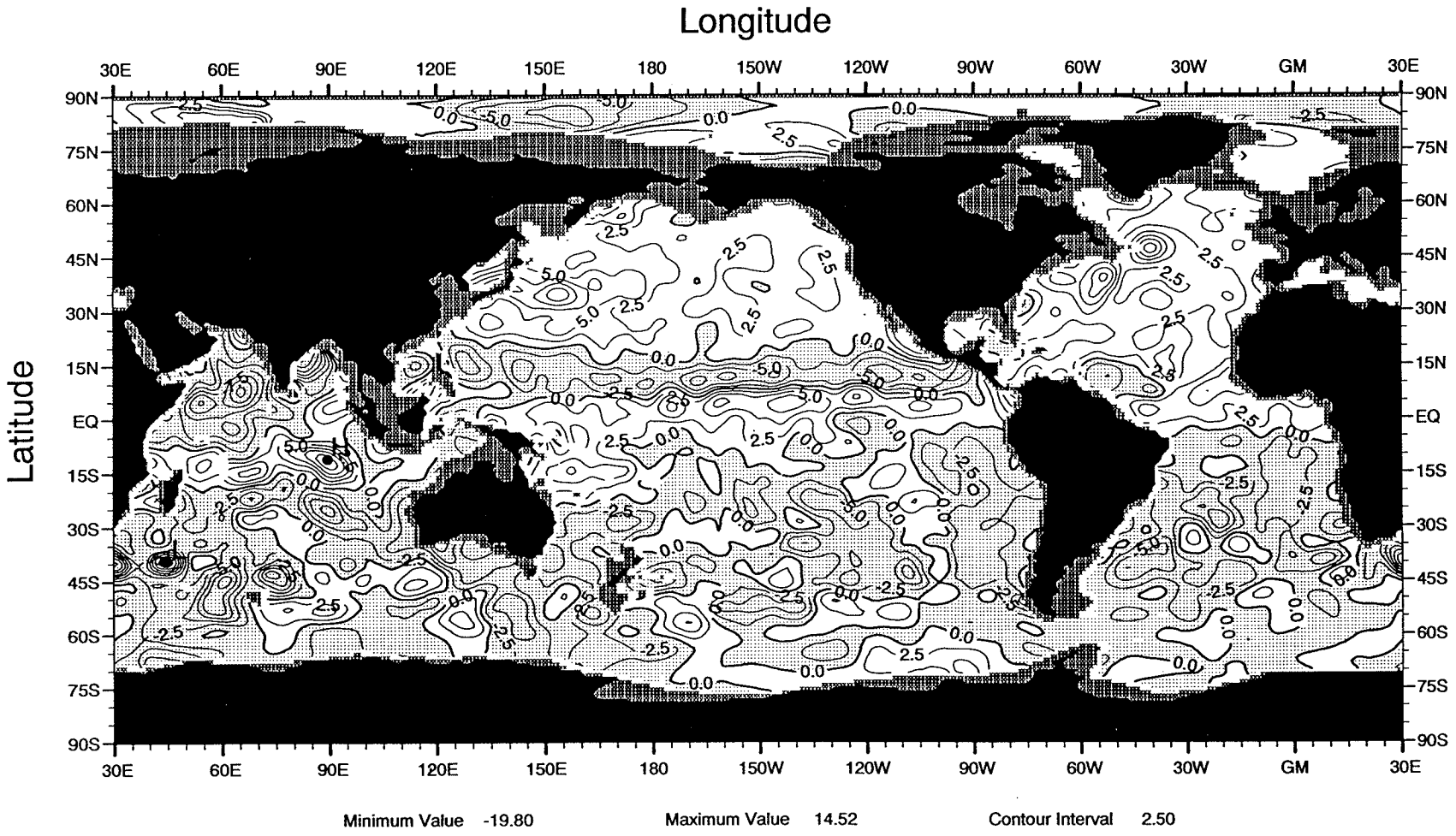

Fig. B11 November mean minus annual mean dynamic height (dynamic cm) 0 - 1000 m

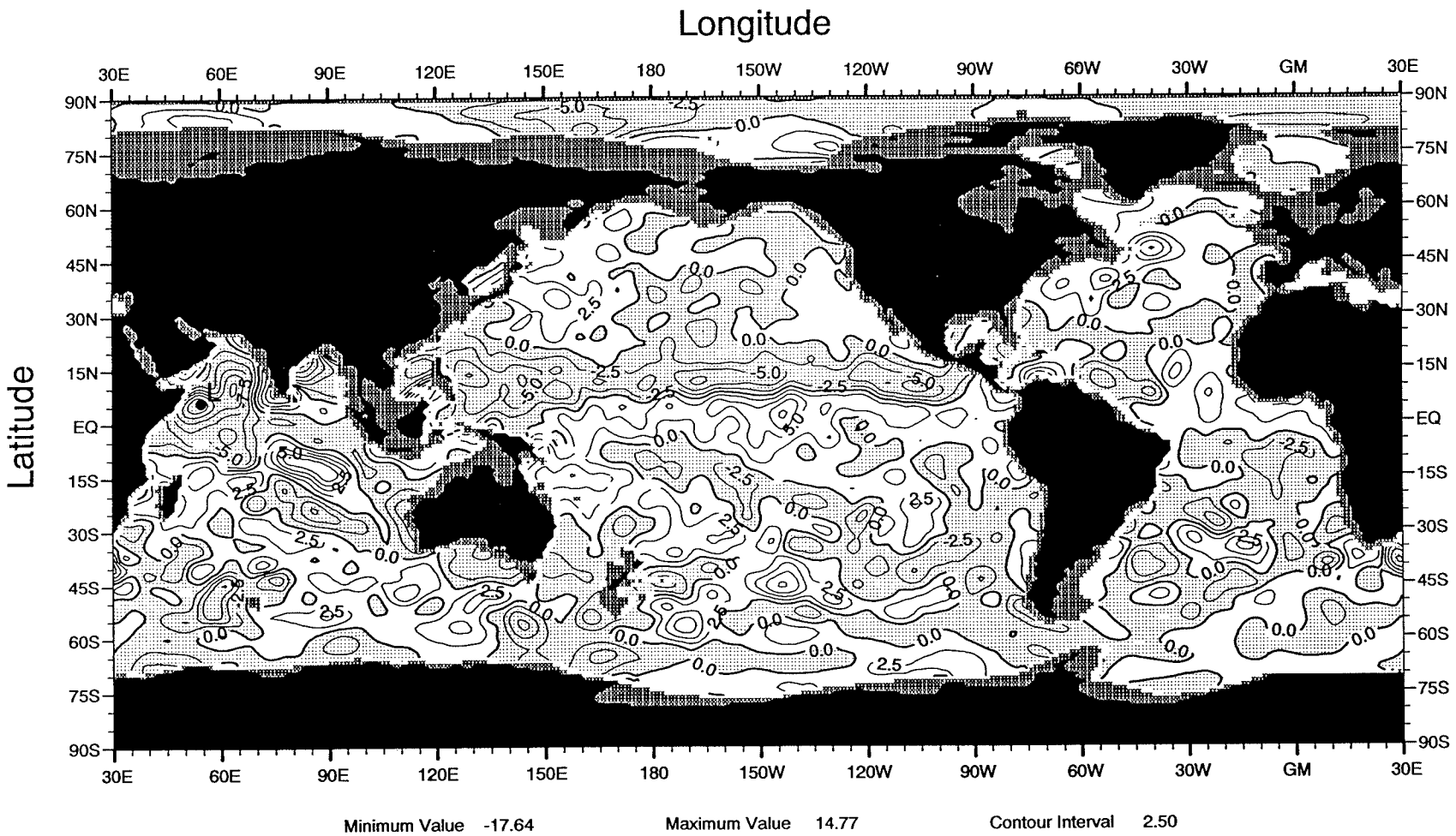

Fig. B12 December mean minus annual mean dynamic height (dynamic cm) 0 - 1000 m

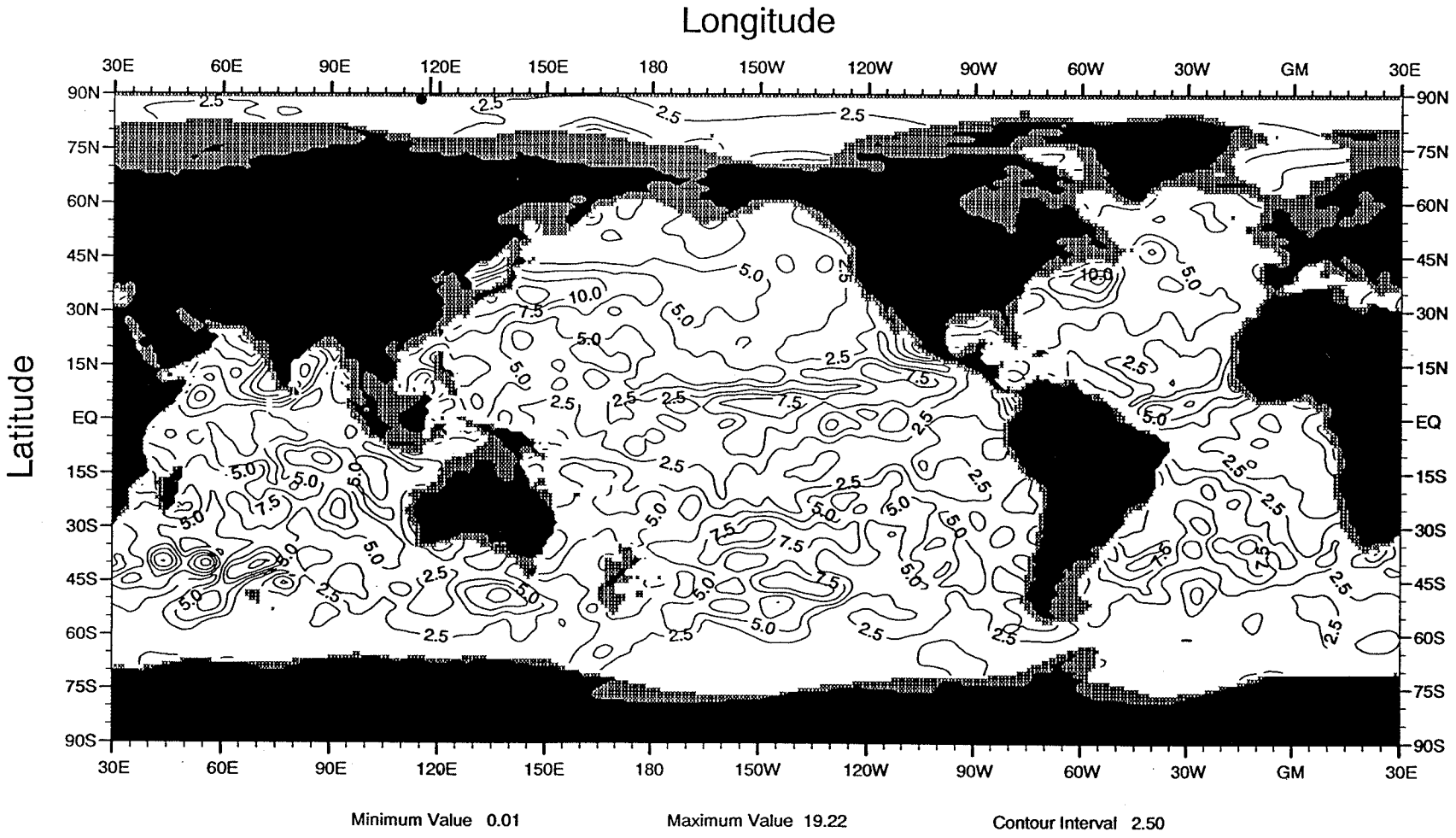

Fig. C1 Amplitude (dynamic cm) of the first harmonic

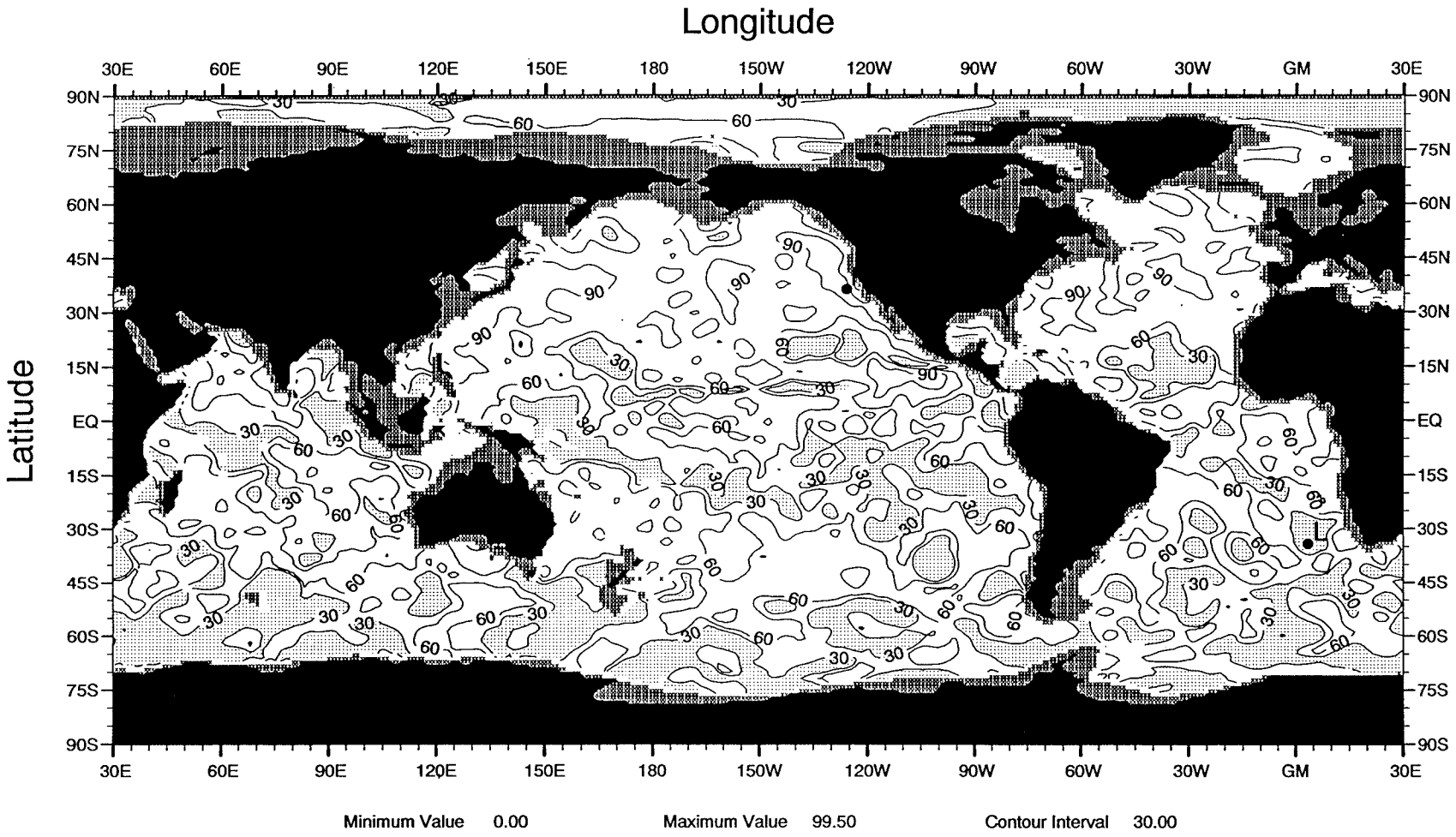

Fig. C2 Percent variance contributed by the first harmonic

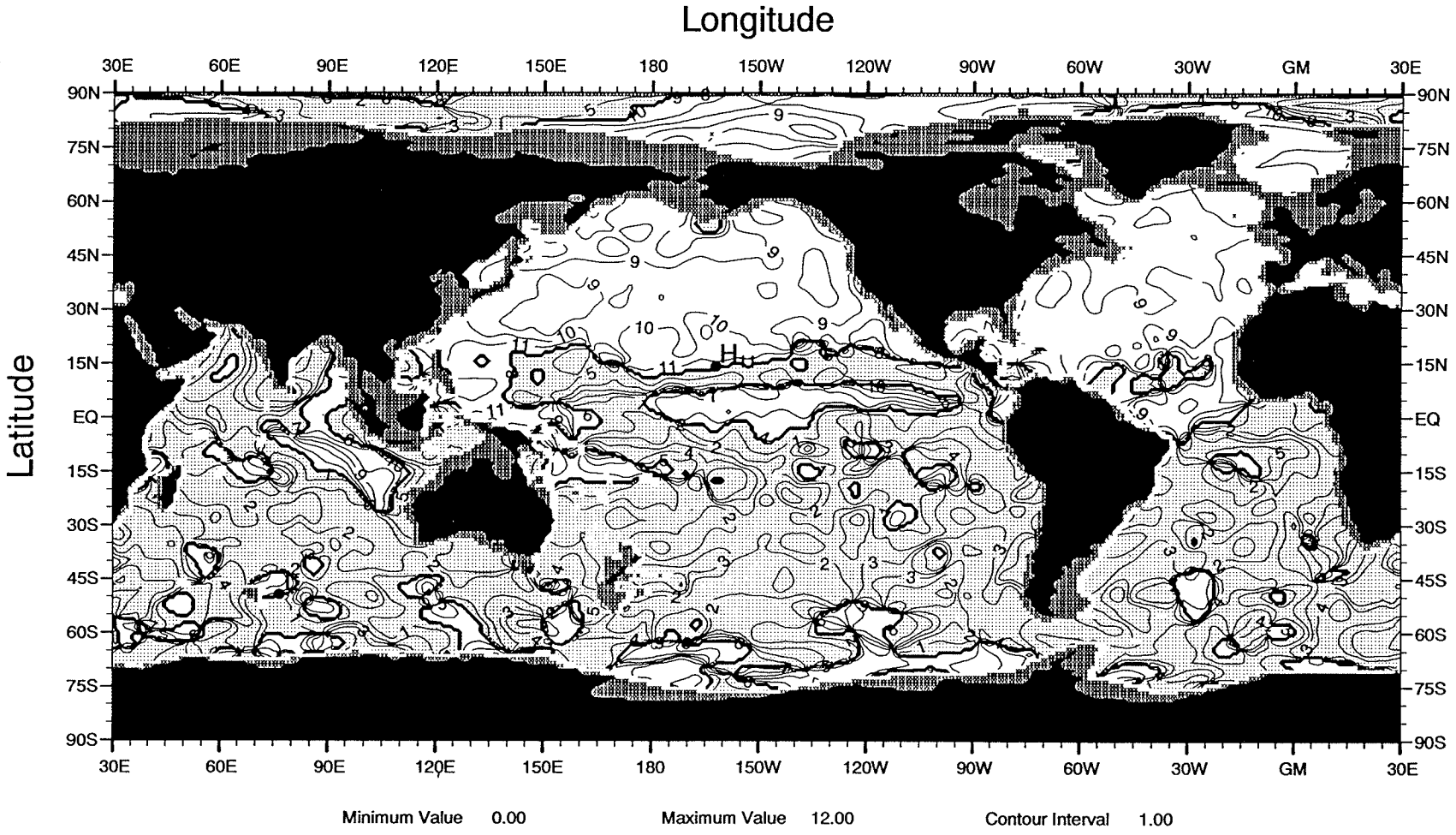

Fig. C3 Phase (months) of the first harmonic

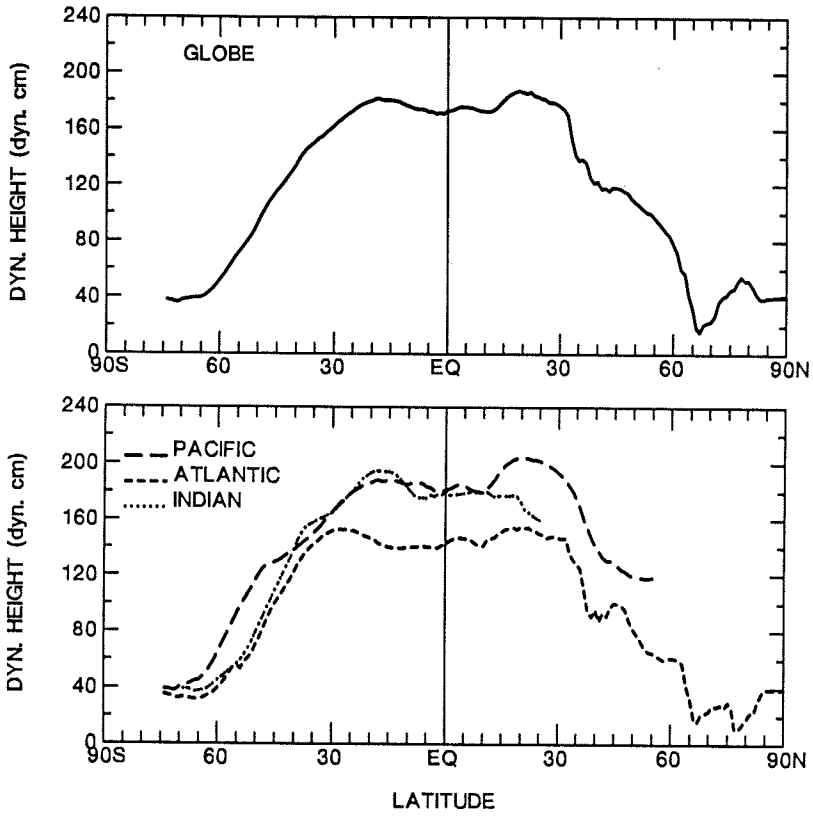

Fig. C4 Zonally averaged annual mean dynamic height (dynamic cm) 0 - 1000 m for the global ocean and individual ocean basins

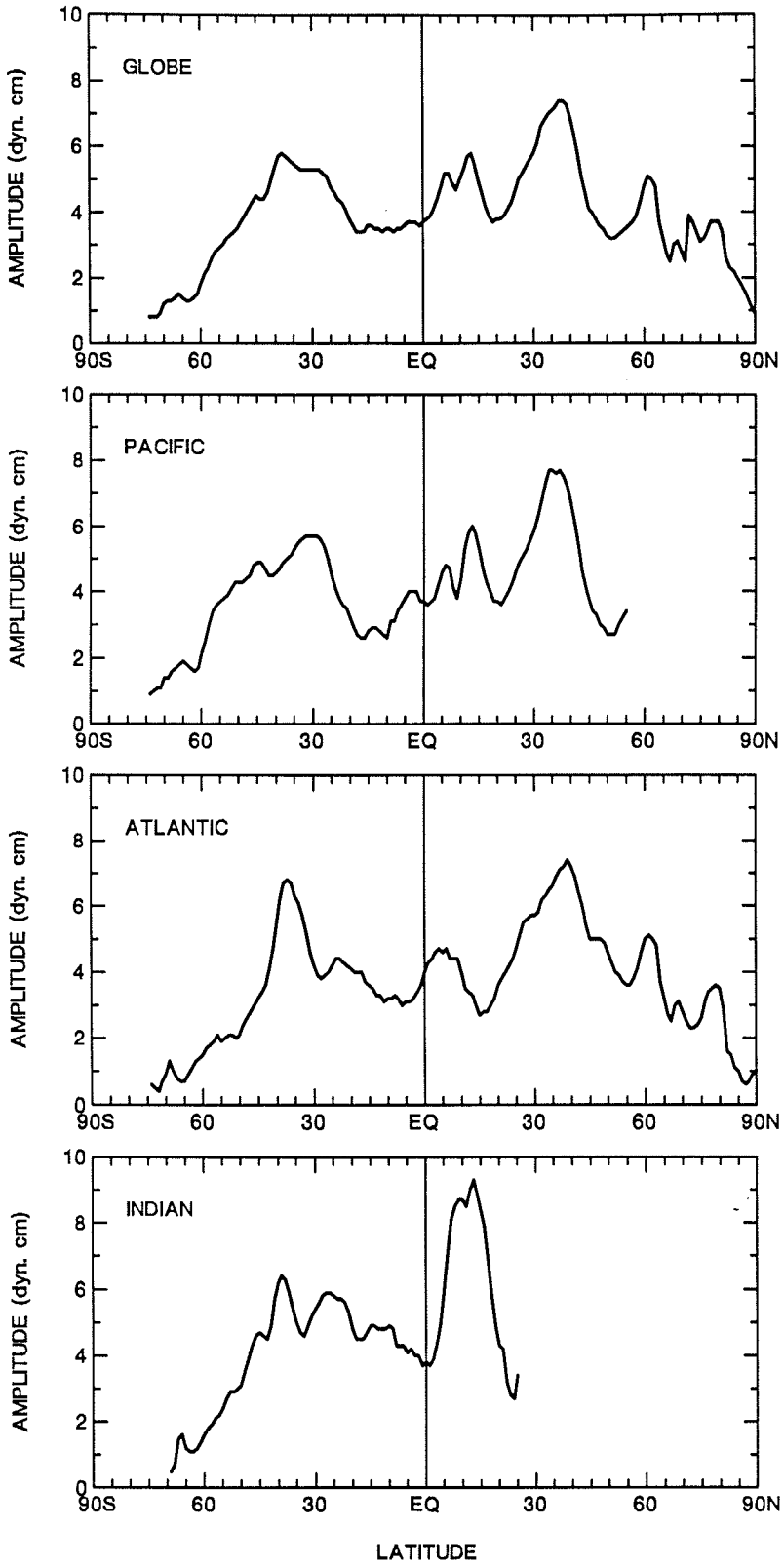

Fig. C5 Zonally averaged amplitude (dynamic cm) of the first harmonic of the climatological annual cycle of dynamic height 0 - 1000 m for the global ocean and individual ocean basins

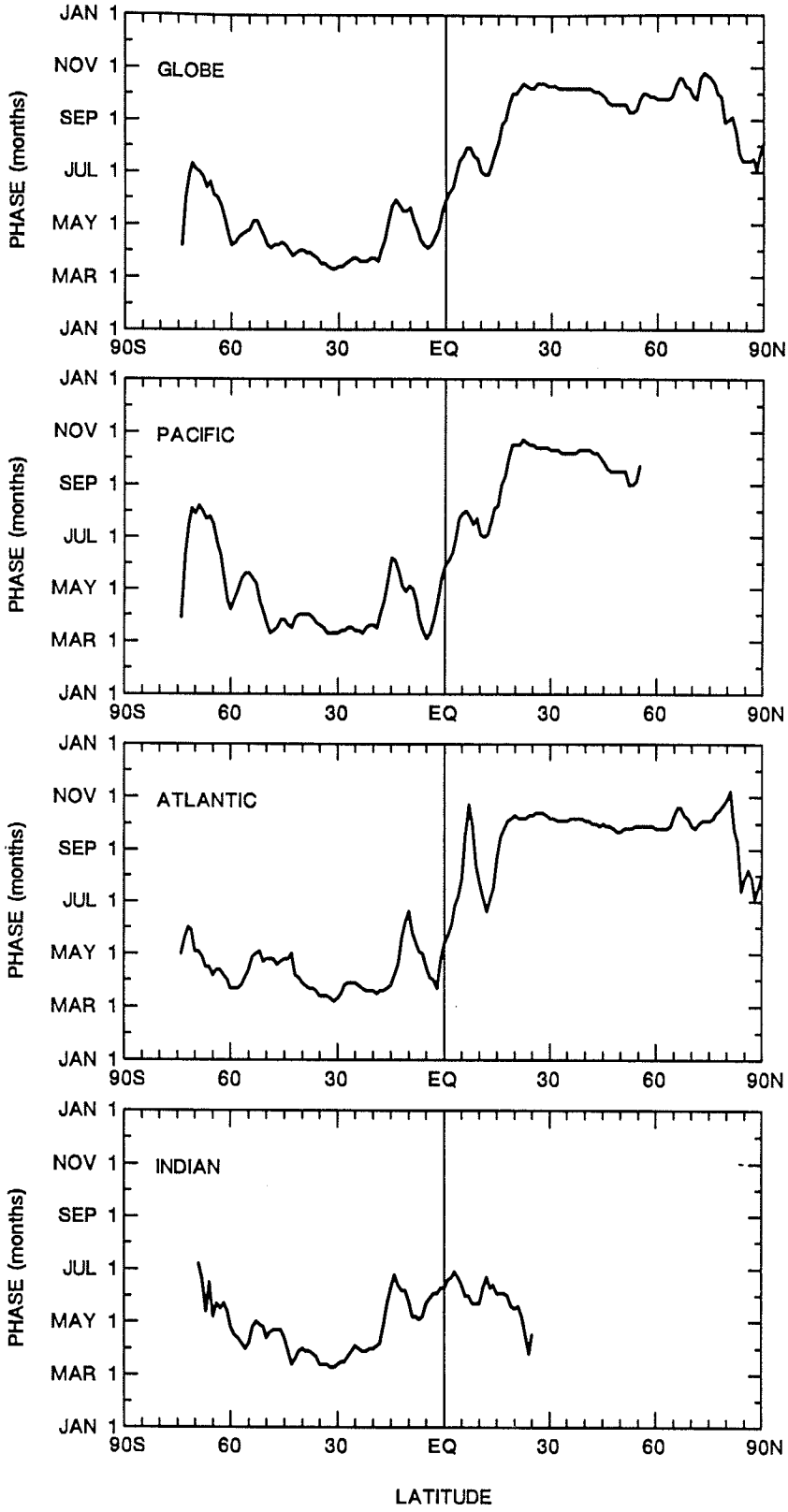

Fig. C6 Zonally averaged phase (months) of the first harmonic of the climatological annual cycle of dynamic height 0 - 1000 m for the global ocean and individual ocean basins

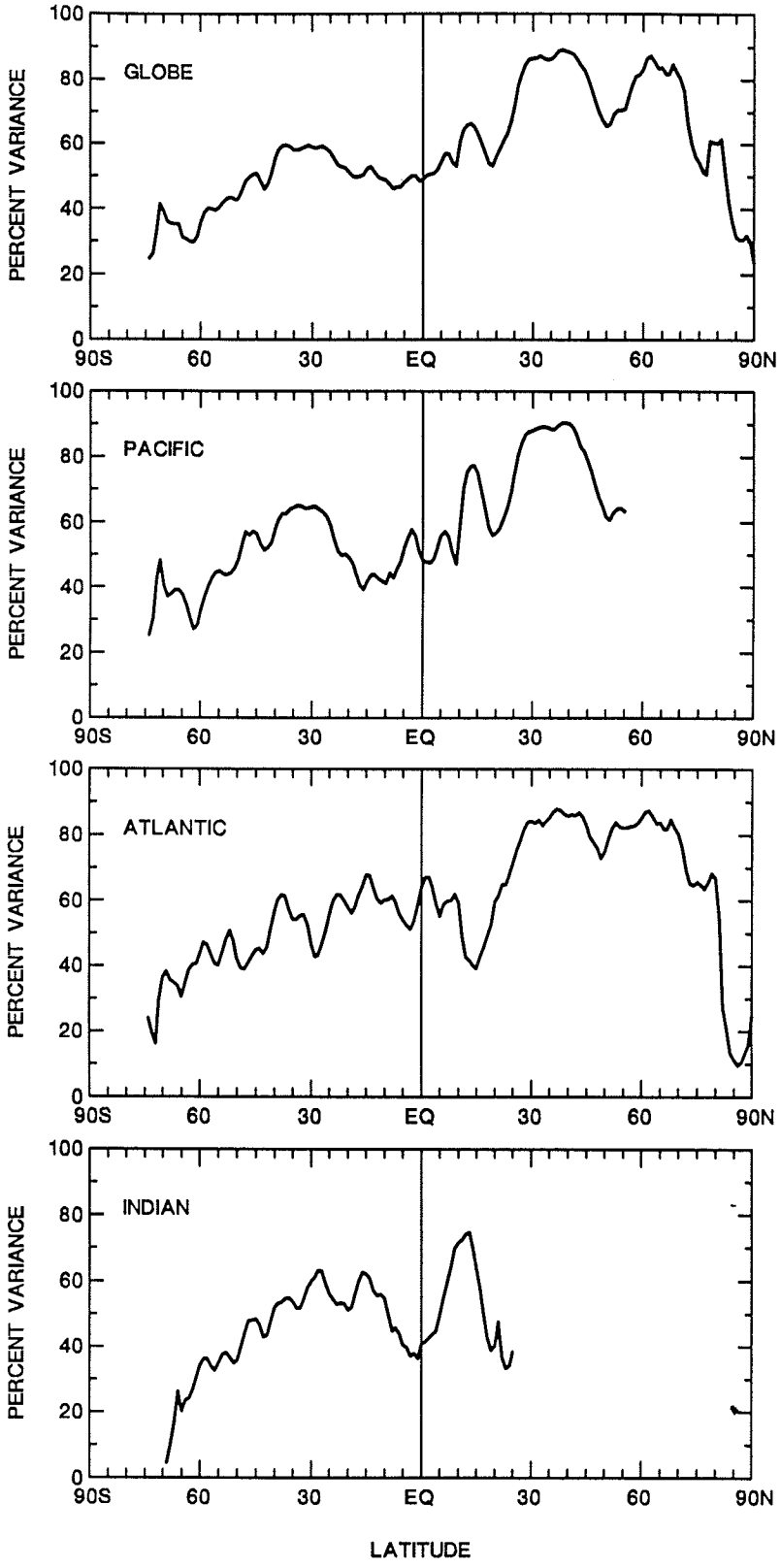

Fig. C7 Zonally averaged percent variance contributed by the first harmonic to the climatological annual cycle of dynamic height 0 - 1000 m for the global ocean and individual ocean basins

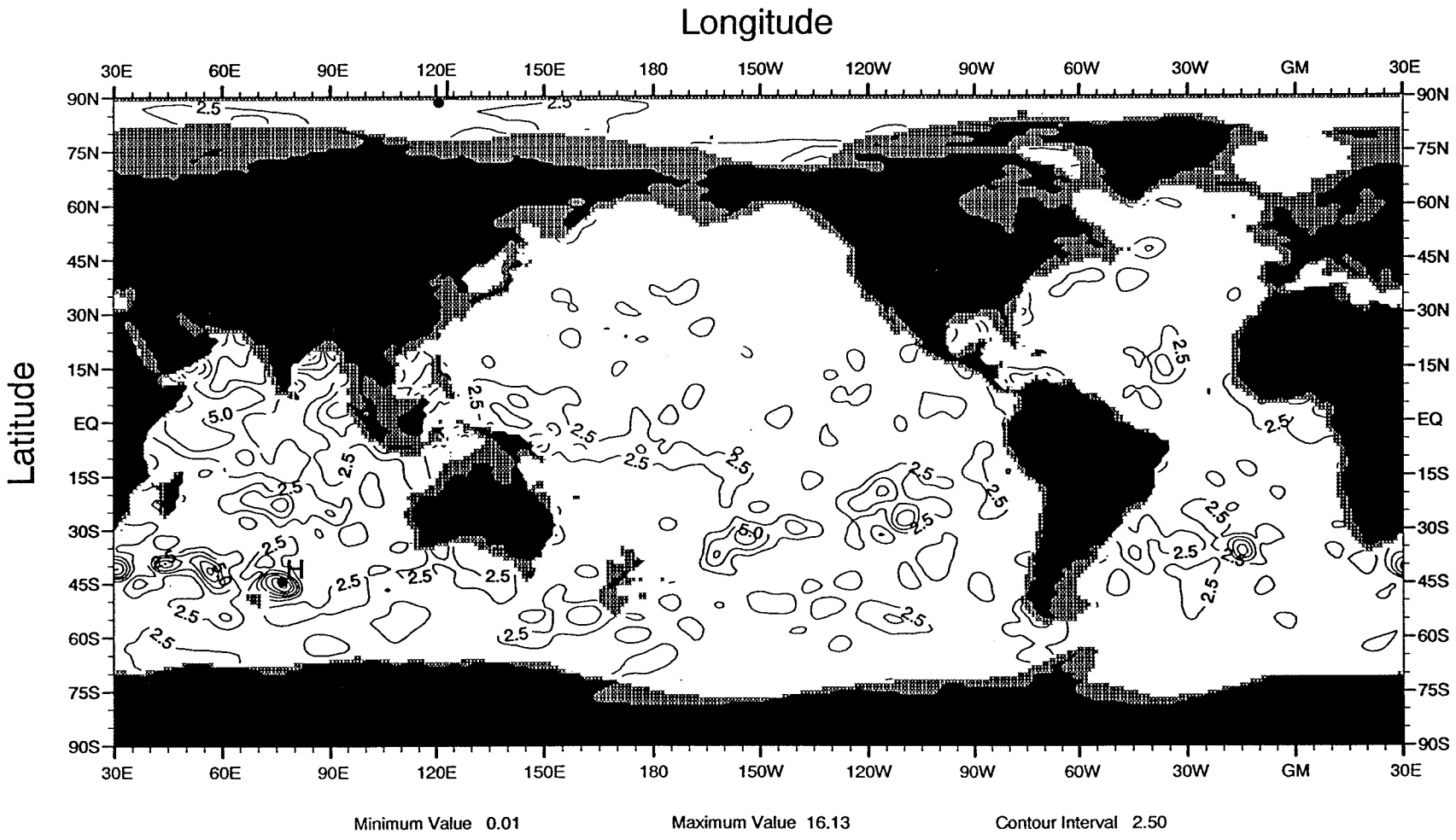

Fig. C8 Amplitude (dynamic cm) of the second harmonic

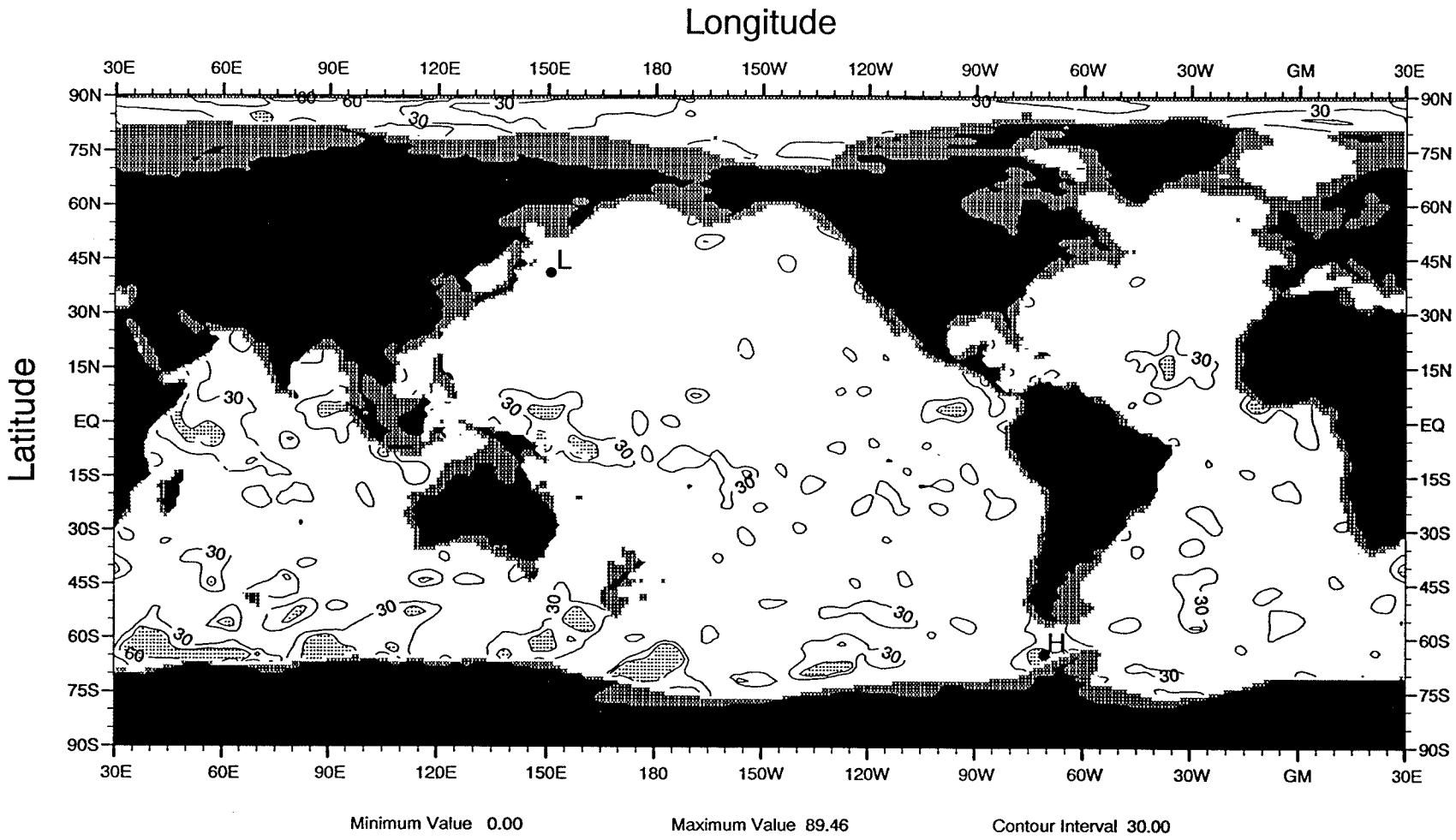

Fig. C9 Percent variance contributed by the second harmonic

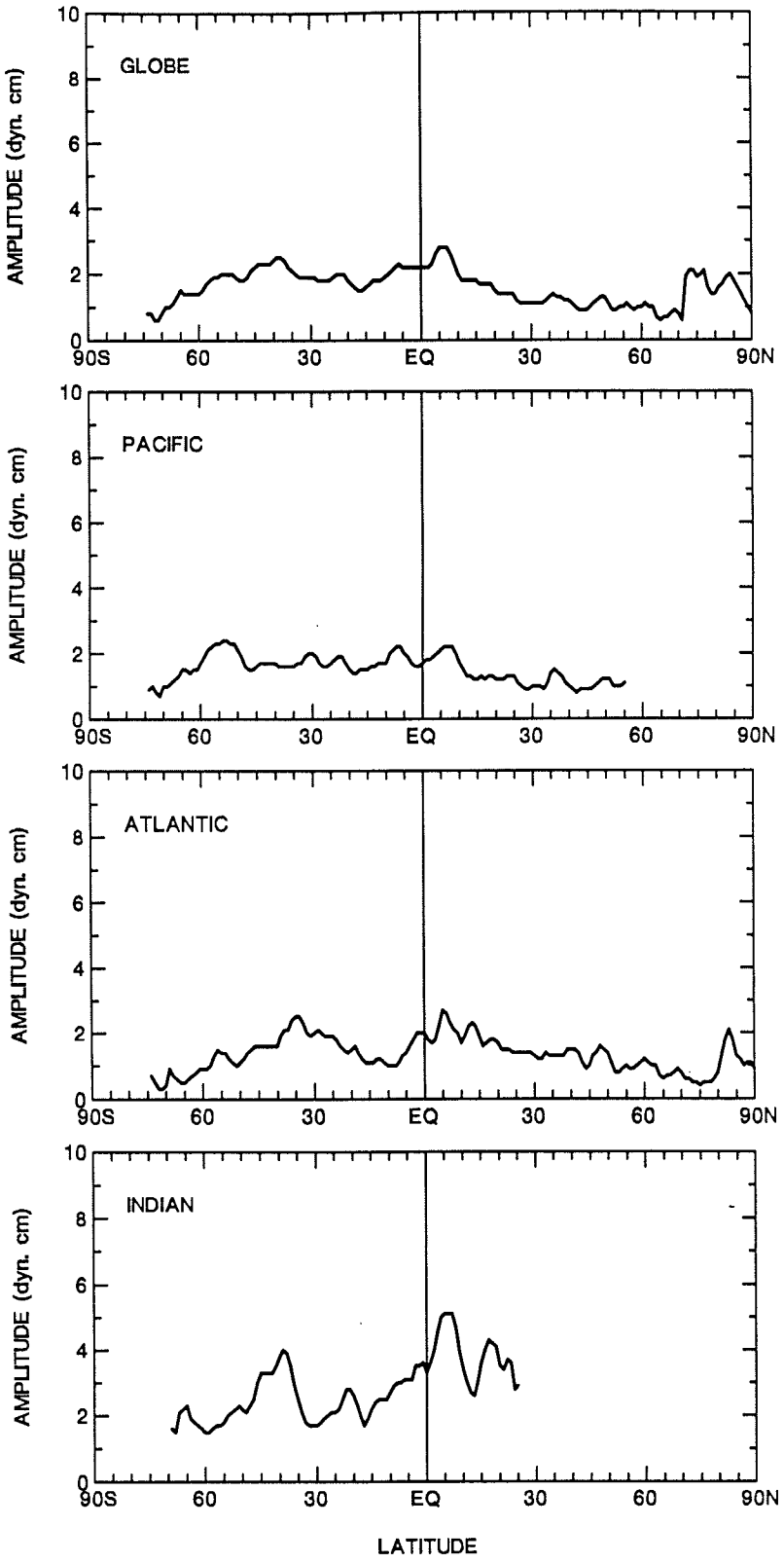

Fig. C10 Zonally averaged amplitude (dynamic cm) of the second harmonic of the climatological annual cycle of dynamic height 0 - 1000 m for the global ocean and individual ocean basins

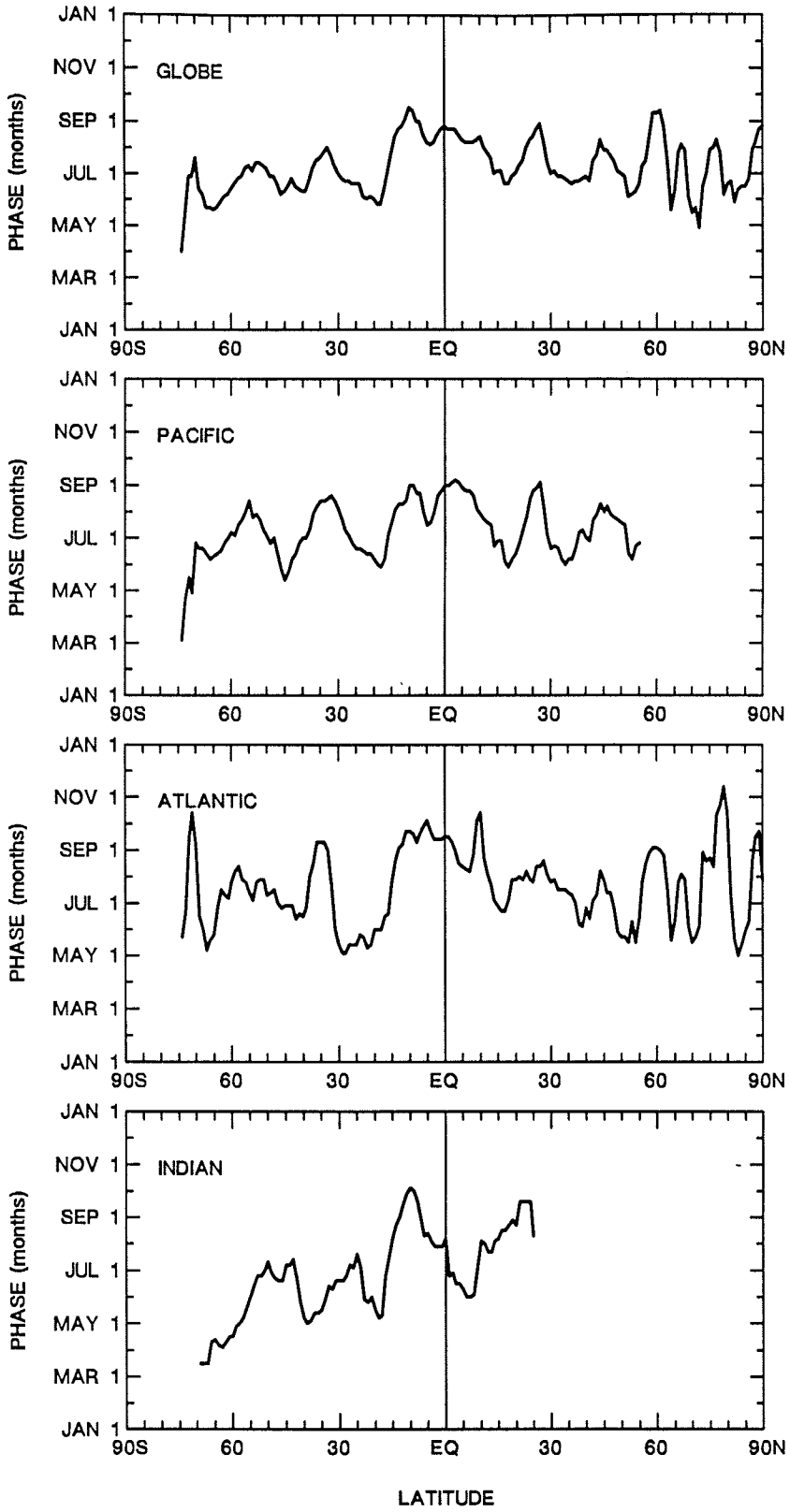

Fig. C11 Zonally averaged phase (months) of the second harmonic of the climatological annual cycle of dynamic height 0 - 1000 m for the global ocean and individual ocean basins

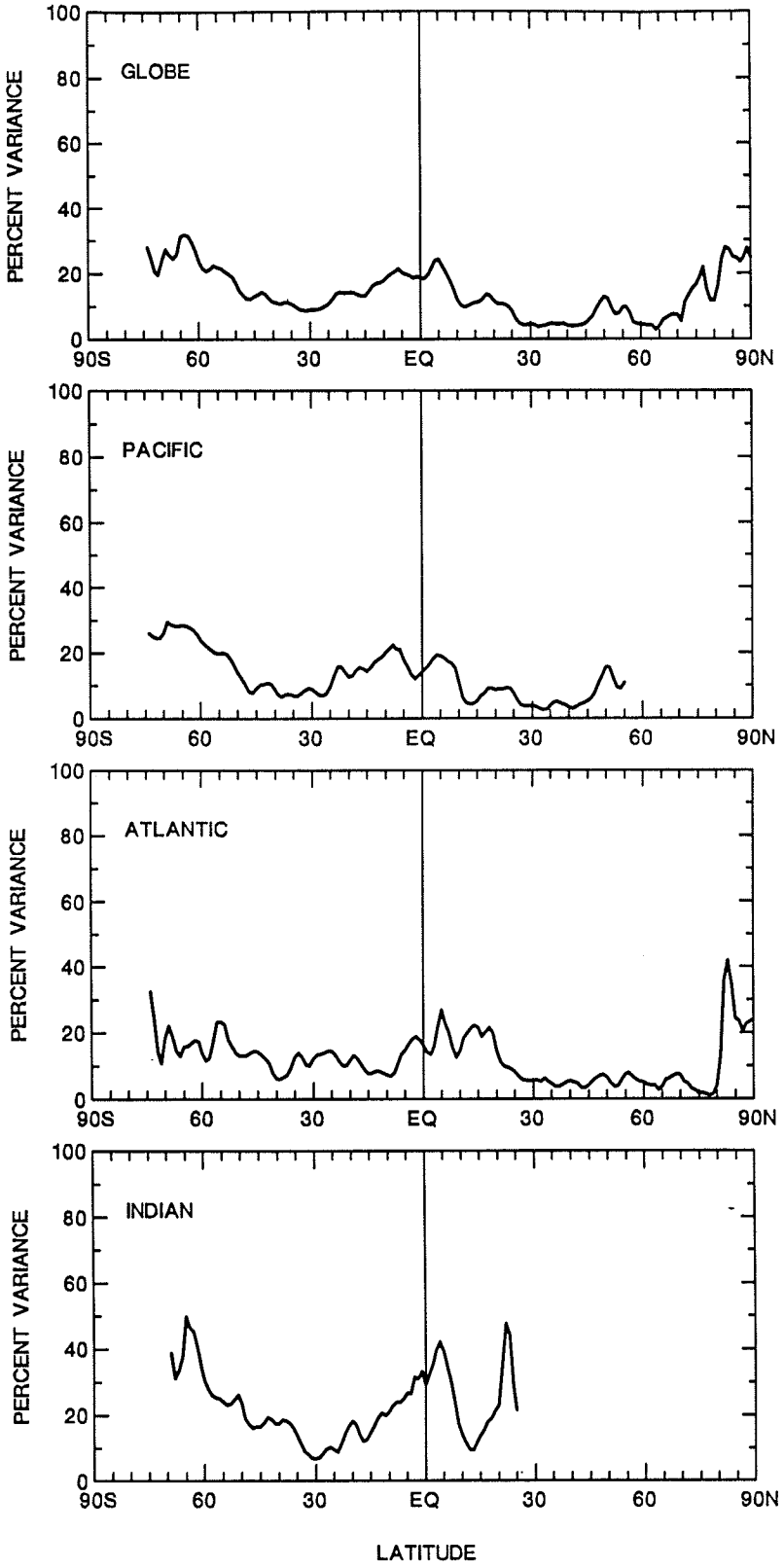

Fig. C12 Zonally averaged percent variance contributed by the second harmonic to the climatological annual cycle of dynamic height 0 - 1000 m for the global ocean and individual ocean basins

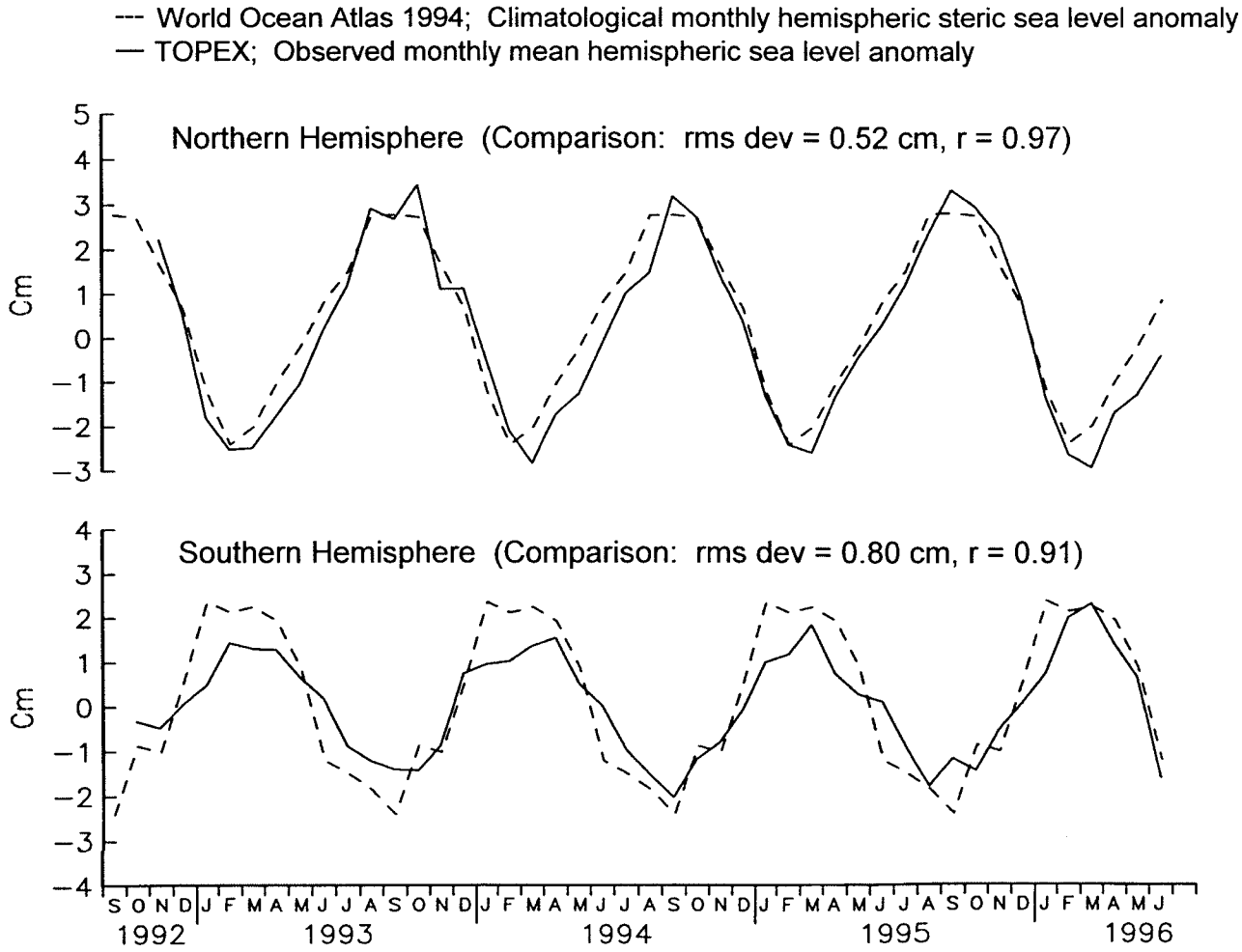

Fig. D1 Hemispheric averages of TOPEX altimeter monthly sea level anomaly (forty-one months) and climatological monthly steric sea level anomaly (deviation from annual mean).

NOAA SCIENTIFIC AND TECHNICAL PUBLICATIONS

The National Oceanic and Atmospheric Administration was established as part of the Department of Commerce on October 3, 1970. The mission responsibilities of NOAA are to assess the socioeconomic impact of natural and technological changes in the environment and to monitor and predict the state of the solid Earth, the oceans and their living resources, the atmosphere, and the space environment of the Earth.

The major components of NOAA regularly produce various types of scientific and technical information in the following kinds of publications:

PROFESSIONAL PAPERS - Important definitive research results, major techniques, and special investigations.

CONTRACT AND GRANT REPORTS - Reports prepared by contractors or grantees under NOAA sponsorship.

ATLAS - Presentation of analyzed data generally in the form of maps showing distribution of rainfall, chemical and physical conditions of oceans and atmosphere, distribution of fishes and marine mammals, ionospheric conditions, etc.

TECHNICAL SERVICE PUBLICATIONS - Reports containing data, observations, instructions, etc. A partial listing includes data serials; prediction and outlook periodicals; technical manuals, training papers, planning reports, and information serials; and miscellaneous technical publications.

TECHNICAL REPORTS - Journal quality with extensive details, mathematical developments, or data listings.

TECHNICAL MEMORANDUMS - Reports of preliminary, partial, or negative research or technology results, interim instructions, and the like.

U.S. DEPARTMENT OF COMMERCE
National Oceanic and Atmospheric Administration
National Environmental Satellite, Data, and Information Service
Washington, D.C. 20233